A Dynamic-Programming Labeling Approach to Hydrogen-Powered Route Selection in Aviation Networks

Lisa-Marie Manke[2,3] Imke Joormann[1,2]

[1] Cluster of Excellence SE^2A—Sustainable and Energy-Efficient Aviation, Technische Universität Braunschweig, 38106 Braunschweig, Germany

[2] Institute of Automotive Management and Industrial Production, Technische Universität Braunschweig, Mühlenpfordtstr. 23, 38106 Braunschweig, Germany

[3] Corresponding author: lisa-marie.manke@tu-braunschweig.de

We study passenger routing in an aviation network that blends hydrogen- and kerosene-powered aircraft. Under our assumptions, hydrogen enables carbon-free short- and medium-haul flights but requires capital-intensive supply facilities, which lead to varying prices and availabilities of hydrogen at specific airports, creating strong interdependencies between routing, technology choice, and infrastructure availability. To capture these trade-offs, we formulate a multi-commodity network-flow model with explicit multi-leg refueling and hydrogen tankering, and we propose an exact dynamic-programming labeling algorithm that exploits network structure to achieve substantial computational gains over general-purpose solvers.

We apply our approach to the European aviation network under varying fuel price and hydrogen supply cenarios, including both heterogeneous and homogeneous cost structures. Results show that hydrogen adoption is strongly driven by fuel costs and cost heterogeneity, increasing from below 0.6 % at low kerosene prices to up to 7.5 % in intermediate and 21.7 % in high-cost scenarios. Although hydrogen-powered flights occur at up to 85 airports, nearly all hydrogen is procured at a handful of supply hubs, demonstrating the critical importance of multi-leg refueling for early-stage infrastructure rollout. Overall, hydrogen aviation emerges as a capacity-constrained network equilibrium in which system-wide feasibility is enabled through transported hydrogen, yet large-scale uptake is bottlenecked by a small set of supply nodes. These insights highlight the critical role of coordinated hub development and flexible routing incentives in accelerating the hydrogen-aviation transition.

Keywords: Hydrogen aviation networks, Multi-commodity network flow, Dynamic-programming labeling algorithm

1 Introduction

Aviation is a cornerstone of global mobility and economic exchange, yet it is also a growing contributor to anthropogenic climate change. The sector currently accounts for approximately 2–3% of global CO_2 emissions, and its relative contribution is expected to increase as other sectors decarbonize more rapidly [20]. Additionally, aviation induces significant non-CO_2 climate effects—such as contrails, cirrus cloud formation, and nitrogen oxide emissions—which may further amplify its climate impact, albeit with considerable uncertainty [5, 22]. These developments underscore the urgency of identifying viable pathways toward net-zero aviation in line with international climate targets.

A range of technological options is currently being explored to decarbonize aviation, including sustainable aviation fuels, battery-electric propulsion, and hydrogen-based concepts [43, 38]. These technologies are likely to play complementary roles across different market segments. Among them, hydrogen has emerged as a promising energy carrier, particularly for short- and medium-range aviation [49]. When used in the form of cryogenic liquid hydrogen (LH_2), it offers the potential to eliminate direct CO_2

emissions and reduce certain non-CO_2 effects [27]. However, its large-scale adoption remains uncertain due to technological, economic, and infrastructural challenges.

Besides the currently missing market-readiness of hydrogen aircraft, one of the central barriers to the development of hydrogen aviation is the need for a dedicated airport-based hydrogen supply infrastructure, including production, liquefaction, storage, and distribution. These investments are capital-intensive and subject to spatial and operational constraints [25]. Moreover, the transition is characterized by strong interdependencies: airlines require reliable hydrogen availability before adopting hydrogen-powered aircraft, while infrastructure providers depend on sufficient demand to justify investments. This interdependence creates a coordination problem that is inherently network-wide.

Despite growing interest in hydrogen aviation, existing studies often focus on individual aspects of the problem, such as aircraft technology design, hydrogen supply and cost modeling, or airport infrastructure planning. While these contributions provide important insights, comparatively few studies adopt an integrated network perspective that jointly considers passenger flow allocation, heterogeneous aircraft technologies with operational constraints, and endogenous hydrogen infrastructure availability at airports. In particular, operational features that become critical under sparse infrastructure conditions—such as multi-leg refueling capabilities enabling aircraft to traverse sequences of non-hydrogen airports—have received limited attention in network-based optimization models. This limits the ability to capture key system interactions and to assess trade-offs between infrastructure deployment, routing decisions, and technology adoption.

To address this gap, we develop an integrated network optimization model that jointly determines passenger flows, aircraft technology usage, and hydrogen infrastructure deployment in an aviation network. The model is formulated as a multi-commodity network flow problem, where each commodity represents passenger demand between an origin–destination (OD) pair. Passenger flows can be routed via itineraries operated by either conventional kerosene-powered or hydrogen-powered aircraft, each incurring different costs and subject to technology-specific constraints, such as range limitations. The objective is to minimize system costs, including flight operating costs and hydrogen production and transportation costs. The model enforces flow conservation for each OD pair and incorporates a market penetration constraint to capture the gradual adoption of hydrogen aircraft. Feasibility of hydrogen operations is ensured through range restrictions and capacity constraints on hydrogen availability at airports.

A key modeling feature is the explicit representation of multi-leg refueling behavior for hydrogen aircraft. Because hydrogen infrastructure is expected to be available only at a subset of airports during early deployment phases, restricting refueling to every stop would require unrealistically dense infrastructure and severely limit feasible routings. By allowing aircraft to carry hydrogen across multiple legs, the model captures operational strategies that enable network connectivity under sparse infrastructure, as considered for example in [37]. This feature substantially increases model complexity, as hydrogen flows must be tracked jointly with passenger flows across multiple flight legs.

To solve the resulting large-scale mixed-integer program, we develop a customized exact dynamic programming labeling algorithm that exploits the problem structure, in particular the limited range of hydrogen aircraft and the sparsity of hydrogen infrastructure. This tailored approach significantly reduces computational effort compared to standard solution methods.

This paper makes the following contributions: First, we develop a network optimization model that jointly captures passenger flow assignment, heterogeneous aircraft technologies, and endogenous hydrogen infrastructure availability, while explicitly incorporating multi-leg hydrogen refueling. This unified formulation enables the analysis of routing, technology choice, and infrastructure constraints within a single framework and allows aircraft operations beyond hydrogen-equipped airports under sparse infrastructure conditions. A simpler version of the model was previously published in the conference proceedings [24].

Second, we propose a customized exact dynamic programming labeling algorithm that exploits key structural properties of the problem, in particular the limited range of hydrogen aircraft and the sparsity of hydrogen supply. While state-of-the-art approaches for multi-commodity network flow problems typically rely on column generation combined with labeling procedures, we show that the specific structure of our problem allows the solution approach to be reduced to a single labeling algorithm. This leads to a significantly more compact and computationally efficient solution method avoiding the need for an explicit master problem.

Finally, we provide computational insights into the interplay between infrastructure availability, operational constraints, and network structure. Our results illustrate how hydrogen infrastructure deployment affects routing patterns, technology adoption, and total system costs, thereby informing strategic planning decisions in the transition toward low-carbon aviation.

The remainder of this paper is structured as follows: The next section reviews the relevant literature. Section 2 introduces the mathematical formulation and Section 3 explains the solution approach. In Section 4, we present the developed case study and compare the computational performance for artificial instances, as well as a discussion of the computational results for the case study. Lastly, Section 5 gives the final conclusions.

1.1 Related Work

The use of hydrogen as an aviation fuel has been studied for several decades; survey papers such as [49] document the breadth of ongoing research and development activities, further underscoring both the momentum in the field and the remaining uncertainties. Early work by Contreras et al. [8] already identified hydrogen as a promising alternative in the context of limited fossil fuel reserves and rising greenhouse gas emissions. More recent research reflects the rapidly growing interest in hydrogen aviation, but also highlights substantial uncertainties regarding its future role. Beyond engineering challenges, the literature addresses a broad range of questions, including the potential for CO_2 emission reductions, the requirements for large-scale infrastructure deployment, and the likely pace and extent of technology adoption. For instance, Sirtori and Trainelli [37] develop an optimization-based framework for integrating hydrogen-powered aircraft into airline networks, introducing the concept of maximum range for single-refueling return trips and demonstrating that strategic fleet assignment and limited hydrogen infrastructure can still enable high network coverage and substantial reductions in climate impact. Yusaf et al. [48] analyze environmental impacts and policy challenges, while Degirmenci et al. [10] provide an overview of infrastructure requirements and the historical development of hydrogen in aviation. A related stream of research focuses on the economic feasibility of hydrogen aviation: Hoelzen et al. [18] estimate hydrogen demand and associated infrastructure costs based on adapted aircraft designs, while Hoelzen et al. [17] analyze the broader business case and identify conditions under which hydrogen-powered aircraft may be cost-competitive. In addition, Oesingmann, Grimme, and Scheelhaase [29] examine global hydrogen demand in aviation and show how regional price differences and aircraft availability can constrain adoption and influence traffic flows.

Only a limited body of work explicitly examines the interaction between hydrogen adoption and flight network design; existing studies primarily address related aspects in isolation. Some contributions integrate hydrogen technologies into network and fleet optimization frameworks, showing that cost heterogeneity and infrastructure configuration play a key role in shaping deployment patterns [30, 4]. Others focus on system-level transition dynamics, emphasizing the importance of technological progress, policy support, and network effects for large-scale adoption [46, 47]. A further line of research highlights the spatial concentration of hydrogen infrastructure around major hubs and its implications for the network structure [21]. Despite these advances, a comprehensive network perspective that jointly captures passenger flows, operational constraints of hydrogen aircraft, and infrastructure availability remains largely unexplored.

Modeling the air transport system via networks is done extensively in the literature—see [50] for an overview—in particular, analyzing the impact of external factors on flight networks: Using a mixed integer optimization approach, [45] focuses on the problem where to introduce hydrogen infrastructure in an existing airline network, together with setting up a new hydrogen-powered fleet. This is achieved via a hub location problem that aims to determine which airports should invest in hydrogen infrastructure in order to maximize the regional covering of hydrogen powered-aviation; in their setting, the option of refueling an aircraft for multiple consecutive flights is not considered. A combination of network modeling and linear optimization techniques for integrating hydrogen-powered aircraft into the European aviation network is presented in [31], assuming a predefined fleet serving origin–destination passenger demand with at most one intermediate stop.

Button [7] evaluates the impact of the liberalization of the international air transport and the removal of economic restrictions on international flight networks. Simulating cost adjustments for specific routes within the European flight network when introducing a European trading scheme for CO_2 emissions is considered in [2]. In [33], the authors investigate how different flight networks that are optimized for less CO_2 emissions, together with aircraft optimized in size and range, effect characteristics like travel time, prices and demand. For a green hub-and-spoke airline network, [39] uses a MILP to jointly optimize network topology, fleet assignment, and environmental impacts—providing methodological parallels to emissions-aware routing with hydrogen aircraft. While not directly considering hydrogen, [28] develop a multi-objective model to jointly optimize airline network topology and operational tactics (e.g., intermediate stopovers, lower flight altitudes) for minimizing climate impact, alongside cost.

These papers typically approach the problem from either a strategic infrastructure planning or system-level emission impact perspective, often relying on relatively static or high-level models. Missing is a network optimization framework that dynamically allocates passenger flows across both kerosene and hydrogen-powered aircraft, while simultaneously accounting for hydrogen availability and aircraft-specific constraints like limited range.

Structurally our problem is modeled via a generalized minimum cost multicommodity flow problem with resource constraints. A review on multicommodity flows including applications and solution methods can be found in [35]. As early as 1970, Cremeans, Smith, and Tyndall [9] used a column generation (CG) approach with a shortest path algorithm for the pricing problem to solve the above problem. A variation of the simplex algorithm, where new columns for the basis are selected via a shortest path algorithm, is proposed in [44]. The current state-of-the-art approach is CG together with a labeling approach for the solution of the pricing problem, as seen in [19] and [42]. The first paper focuses on additional constraints on paths within the model, whereas the second paper has a specific application in liner shipping. Considering a dynamic graph computing model, [13] proposes a path selection algorithm on evolving networks. Alvelos and de Carvalho [3] introduce a cycle-based formulation for multicommodity network flow problems on planar graphs and develop a CG framework combined with partitioning techniques to effectively solve large-scale instances with multiple flow types.

Algorithmically, our approach builds on exact dynamic programming labeling algorithms. The foundations of dynamic programming trace back to Bellman [6], while early labeling methods for shortest path problems were introduced by Dijkstra [12]. These ideas were later extended to the shortest path problem with resource constraints (SPPRC) by Desrochers [11] and to its elementary variant by Feillet et al. [14]. In modern network optimization, labeling algorithms are predominantly embedded within branch-and-price frameworks, where column generation relies on solving SPPRC-type pricing problems. This paradigm has been successfully applied to a variety of routing problems, where advanced acceleration techniques such as bidirectional labeling, ng-neighborhood relaxations, and heuristic pricing are crucial for computational efficiency [34]. However, the literature also highlights important limitations of classical labeling approaches. In particular, the presence of complex resource interdependencies can significantly weaken dominance rules and lead to an almost complete enumeration of labels, rendering standard labeling schemes ineffective [40]. Similarly, for highly constrained variants such as the soft-clustered vehicle routing problem, even state-of-the-art labeling algorithms become computationally prohibitive, motivating alternative pricing approaches based on integer programming [16]. More recent contributions demonstrate that labeling algorithms can be extended to incorporate additional problem features, such as robustness with respect to uncertainty, by embedding these aspects directly into the resource extension functions [26].

Motivated by these developments, we propose a tailored labeling algorithm for a multi-commodity flow problem that explicitly accounts for commodity-specific resource interactions within the labeling process. In contrast to classical SPPRC settings, the multi-commodity structure introduces additional coupling constraints across flows, which necessitates refined state representations and dominance criteria to ensure tractability. Our approach extends the traditional labeling framework to efficiently capture these interdependencies while maintaining computational performance.

2 Hydrogen Aviation Network Problem

Determining where to integrate hydrogen-powered aircraft into the existing aviation system—and how to modify current flight path networks to accommodate their unique range and seating capacities—is a complex challenge. This section introduces a mixed-integer linear program (MILP) designed to identify a cost-optimal solution to these integration and routing decisions.

We model the aviation network as a bidirectional graph $G = (V, A)$, where V denotes the set of airports and A the set of possible flight connections. Each arc $a \in A$ can be operated using hydrogen- or kerosene-powered aircraft. Kerosene operation is characterized solely by cost per arc and per passenger, and is assumed to be unconstrained in terms of fuel availability. In contrast, hydrogen-powered operation is subject to range and supply limitations.

Let $\{(O_1, D_1), \ldots, (O_N, D_N)\}$, with $N \in \mathbb{N}$, denote the set of origin–destination (OD) pairs representing multiple commodities, each corresponding to an estimated passenger demand d_i in the considered aviation system. This demand can be served by hydrogen-powered aircraft or by aircraft fueled with kerosene. To model this, we introduce two separate flow types for each OD pair: one for hydrogen-powered transport and one for kerosene-fueled transport. Flow in this context can be interpreted either as the estimated number of aircraft operating on this flight path or as the estimated number of passengers who want to travel from the origin to the destination. In this work, we adopt the latter interpretation, considering flow as passenger demand.

For $n \in \mathbb{N}$, we define $[n] := \{1, 2, \ldots, n\}$, and let $i \in [N]$ index the commodities. For $u, v \in V$, let $[u, v]$ denote the commodity from u to v. Let $\omega \in \{h, k\}$ denote the fuel type, where h refers to hydrogen and k to kerosene. We define flow functions $f_i^\omega : \mathcal{P}(A) \to \mathbb{R}_{\geq 0}$, which map subsets of A to non-negative real numbers, representing the aggregated flow of commodity i using fuel type ω over each arc. We model these flow variables as continuous rather than integer-valued variables, since the corresponding flow quantities in the relevant instances are typically very large. Consequently, the expected rounding error is negligible, while the continuous formulation significantly reduces the computational complexity of the model. In other words, $f_i^\omega(a)$ denotes the total flow of commodity i using fuel type ω that traverses an arc set $A' \subseteq A$,

$$f_i^\omega(A') = \sum_{a \in A'} \varphi_i^\omega(a),$$

where $\varphi_i^\omega(a)$ is the flow value on arc $a \in A$.

To formulate the constraints governing passenger flow, let $\delta^+ : V \to \mathcal{P}(A)$ and $\delta^- : V \to \mathcal{P}(A)$ be the functions assigning its set of outgoing and ingoing arcs to each vertex, respectively. First, we define flow conservation constraints to ensure that the total number of passengers transported between each origin–destination pair matches the specified demand,

$$\begin{aligned} f_i^h(\delta^+(O_i)) + f_i^k(\delta^+(O_i)) &= d_i + f_i^h(\delta^-(O_i)) + f_i^k(\delta^-(O_i)) \qquad \forall i \in [N] \\ f_i^h(\delta^-(D_i)) + f_i^k(\delta^-(D_i)) &= d_i + f_i^h(\delta^+(D_i)) + f_i^k(\delta^+(D_i)) \qquad \forall i \in [N]. \end{aligned}$$

Here, d_i denotes the estimated demand for commodity $i \in [N]$. Next, we impose flow conservation constraints on each intermediate vertex to ensure that passenger flow is preserved across the network, such that each passenger ultimately reaches their designated destination,

$$f_i^h(\delta^+(v)) + f_i^k(\delta^+(v)) = f_i^h(\delta^-(v)) + f_i^k(\delta^-(v)) \qquad \forall v \in V \setminus \{O_i, D_i\} \ \forall i \in [N].$$

Since no hydrogen-powered commercial aircraft are currently in operation and their market introduction is expected to occur in the future [1], it is necessary to account for the limited availability of hydrogen-powered aircraft in the model,

$$f_i^h(\delta^+(O_i)) \leq Q d_i \qquad \forall i \in [N],$$

such that the hydrogen-powered flow cannot exceed an explicit upper bound given by the market penetration Q. In this context, market penetration refers to the proportion of hydrogen-powered aircraft within the total operational fleet. Since our model does not explicitly represent individual aircraft, we approximate this value by applying the penetration rate to passenger flows instead.

A further critical aspect in addressing the above questions is the availability of hydrogen. Let $\mathcal{T}$ denote the transportable hydrogen amount per passenger, obtained by dividing the estimated tank size of a hydrogen-powered aircraft by its seating capacity. For each arc a, we define r_a as the hydrogen consumption per passenger for operating the arc with a hydrogen-powered aircraft. An arc is feasible for hydrogen-powered operation if $r_a \leq \mathcal{T}$. In addition, each airport v provides only a limited hydrogen supply, denoted by $\mathcal{H}_v$, with hydrogen costs assumed to be airport-specific.

Since hydrogen production is highly energy-intensive and its sustainability depends on regional availability of renewable energy, both the quantity and cost of hydrogen may differ between airports. This spatial heterogeneity can incentivize strategies such as refueling for multiple subsequent flights at airports with lower hydrogen prices, thereby reducing operational costs and enabling hydrogen-powered operation on routes that would otherwise be infeasible. To capture this behavior within the model, it is necessary to track the portion of hydrogen-powered demand on each arc that is supplied by hydrogen not procured at the arc's source airport. To facilitate this, we introduce the concept of hydrogen excess paths, which represent paths over which hydrogen is carried from a source to a destination, where it can then be used on outgoing arcs.

Definition 2.1 (Hydrogen Excess Path)**.** *Let $p = (a_1, \ldots, a_M)$ be a path in G with $M \geq 1$. Let $\hat{\mathcal{T}}^p := \mathcal{T} - \sum_{j=1}^{M} r_{a_j}$ be a so called **transport capacity** at the target of a_M. Then p is a **hydrogen***

excess path *if and only if* $\hat{\mathcal{T}}^p > 0$ *holds. Let* P^{ex} *be the set of all hydrogen excess paths in* G.

Outgoing arcs of the target of $a_M = (u, v)$ are called outgoing arcs of p; for better readability let $\delta^+(p) := \delta^+(v)$.

For each hydrogen excess path $p \in P^{ex}$ and arc $a \in \delta^+(p)$, let t_a^p be the amount of flow on arc a that is operated at least partially using hydrogen originating from the transport capacity of path p. Capturing this requires not only the proportion of demand served by hydrogen-powered aviation, but also the distribution of hydrogen usage across arcs. To model this, we introduce two types of variables related to hydrogen usage. The first, $h_a \in \mathbb{R}_{\geq 0}$ for all $a \in A$, denotes the amount of hydrogen purchased at the source airport of arc a and directly used to operate a. The second type, $h_a^p \in \mathbb{R}_{\geq 0}$, is defined for all hydrogen excess paths $p \in P^{ex}$ and arcs $a \in \delta^+(p)$. This variable represents the quantity of hydrogen purchased at the source of path p that remains unused on all arcs on p and is therefore available for use on arc a.

To incorporate hydrogen-related constraints into the network model, we begin by introducing an inequality that limits the amount of hydrogen that can be purchased at each airport v,

$$\sum_{a \in \delta^+(v)} h_a + \sum_{a \in \bigcup_{p \in P_v} \delta^+(p)} h_a^p \leq \mathcal{H}_v \qquad \forall v \in V.$$

Here, $P_v \subseteq P^{ex}$ denotes the set of hydrogen excess paths beginning in the vertex $v \in V$. There is also a limit on the amount of hydrogen that can be carried on each flight,

$$h_a + \sum_{p: a \in \delta^+(p)} h_a^p + \sum_{e \in \bigcup_{p \in P_a} \delta^+(p)} h_e^p \leq \mathcal{T} \sum_{i \in [N]} f_i^h(a) \qquad \forall a \in A,$$

where $P_a \subseteq P^{ex}$ denotes the set of all hydrogen excess paths that begin with arc $a \in A$. This constraint ensures that the total hydrogen required to operate arc a, along with the hydrogen carried for future use, does not exceed the amount of hydrogen transportable per passenger $\mathcal{T}$. Specifically, the second term captures the hydrogen used from a transport capacity at the source of a, while the third term accounts for hydrogen purchased at the source of a intended for later use. It is then necessary to ensure that each flight is loaded with sufficient hydrogen, which leads to the following constraint:

$$h_a + \sum_{p: a \in \delta^+(p)} h_a^p \geq r_a \sum_{i \in [N]} f_i^h(a) \qquad \forall a \in A.$$

As outlined earlier, the objective is to minimize the total operating cost of all flights in the reconfigured flight network. To this end, let c_a^m denote the non-fuel direct operating cost per arc $a \in A$ and per passenger for hydrogen-powered aircraft. Let c_v^h represent the cost of hydrogen at airport $v \in V$. We assume that kerosene prices are uniform across all airports, so cost variations for kerosene operations arise solely from differences in arc lengths. Let c_a^k denote the total cost per arc and per passenger for kerosene-powered flights, including non-fuel direct operating cost.

Our model should exclude solutions that reroute commodities along inferior paths solely to generate transport capacity for other commodities. Such reroutings are of limited practical relevance, as passengers are unlikely to accept significant detours merely to enable the use of cheaper hydrogen for others. Furthermore, these reroutings often lead to inefficient resource utilization due to the additional transport effort associated with long detours. To this end, let C_i denote the cost for the amount of hydrogen required to operate commodity $i \in [N]$ purchased at the origin of i on its direct route using hydrogen-powered aircraft, including the cost for non-fuel direct operation per arc c_a^m; $\tilde{R}_i$ be the amount of hydrogen needed to operate the direct route for commodity i; and $\mathcal{R} := \{i \in [N] : \sum_{j \in [N]: O_j = O_i} \tilde{R}_j d_j \leq \mathcal{H}_{O_i}\}$ be the set of all commodities which start in vertices that provide enough hydrogen capacity to operate all outgoing commodities by hydrogen. Let $s(a)$ denote the source of arc a. Then

$$\sum_{a \in A} (\min\{c_{O_i}^h, c_{s(a)}^h, \min_{\tilde{a} \in P_{s(a)}} c_{s(\tilde{a})}^h\} \cdot r_a + c_a^m) f_i^h(a) \leq C_i d_i \qquad \forall i \in \mathcal{R}$$

ensures that the total hydrogen consumption associated with commodity i does not exceed the amount required on its direct hydrogen-powered route. Consequently, commodities in $\mathcal{R}$ cannot be rerouted along longer hydrogen-powered paths merely to create additional transport capacity for other commodities. The restriction is applied only to commodities in $\mathcal{R}$, since for all other commodities the limited hydrogen availability at the origin airport already constitutes the binding constraint. As a result, rerouting such commodities cannot be used to create economically advantageous transport capacities, and the undesirable detour effect addressed by the constraint cannot occur. Additionally, commodities outside $\mathcal{R}$ could benefit from using hydrogen from a transport capacity coming from airports with higher costs than their origin.

Finally, our model should account for the possibility of refueling a hydrogen-powered aircraft for multiple subsequent flights. To this end, several characteristics of the refueling process must be incorporated. In particular, we prohibit empty flights. This means that the amount of hydrogen flow on an arc that uses transport capacity cannot exceed the amount of hydrogen flow on the respective hydrogen excess path from this transport capacity, leading to

$$\sum_{a \in \delta^+(v)} t_a^p \leq \sum_{i \in [N]} f_i^h(a') \qquad \forall v \in V \ \forall p \in P^v \ \forall a' \in p,$$

where $P^v \subseteq P^{ex}$ denotes the set of all hydrogen excess paths in G which are ending in $v \in V$. Furthermore, for each arc $a \in A$, we impose a constraint to ensure that the portion of demand utilizing transport capacity does not exceed the actual hydrogen-powered demand on arc a,

$$\sum_{p: a \in \delta^+(p)} t_a^p \leq \sum_{i \in [N]} f_i^h(a) \qquad \forall a \in A.$$

Lastly, refueling an aircraft from another aircraft must not be permitted. Since individual aircraft are not explicitly tracked in our model, this restriction has to be enforced indirectly through the passenger flows that generate transport capacity. To this end, we require t_a^p to be integer-valued. This prevents transport capacities generated by different passengers from being artificially aggregated into fractional capacities that could subsequently be used to enable hydrogen transport in a way that would not correspond to any feasible aircraft operation. In particular, the integrality of t_a^p prevents the implicit merging of transport capacities originating from different hydrogen excess paths, which would effectively amount to allowing aircraft-to-aircraft refueling. Additionally, we constrain the amount of hydrogen using a specific transport capacity to be a multiple of this transport capacity,

$$h_a^p \leq \hat{\mathcal{T}}^p t_a^p \qquad \forall p \in P^{ex} \ \forall a \in \delta^+(p).$$

Combining these elements yields the MILP-formulation of the Hydrogen Aviation Network Problem (HANP):

$$\begin{aligned}
\min \sum_{i \in [N]} \left(\sum_{a \in A} c_a^m f_i^h(a) + \sum_{a \in A} c_a^k f_i^k(a) \right) + \sum_{v \in V} c_v^h \sum_{a \in \delta^+(v)} h_a & \\
\text{s.t.} \quad f_i^h(\delta^+(O_i)) + f_i^k(\delta^+(O_i)) = d_i + f_i^h(\delta^-(O_i)) + f_i^k(\delta^-(O_i)) & \quad \forall i \in [N] \quad (1) \\
f_i^h(\delta^-(D_i)) + f_i^k(\delta^-(D_i)) = d_i + f_i^h(\delta^+(D_i)) + f_i^k(\delta^+(D_i)) & \quad \forall i \in [N] \quad (2) \\
f_i^h(\delta^+(v)) + f_i^k(\delta^+(v)) = f_i^h(\delta^-(v)) + f_i^k(\delta^-(v)) & \quad \forall v \in V \setminus \{O_i, D_i\} \ \forall i \in [N] \quad (3) \\
f_i^h(\delta^+(v)) \leq Q d_i & \quad \forall i \in [N] \quad (4) \\
\sum_{a \in \delta^+(v)} h_a + \sum_{a \in \bigcup_{p \in P_v} \delta^+(p)} h_a^p \leq \mathcal{H}_v & \quad \forall v \in V \quad (5) \\
h_a + \sum_{p: a \in \delta^+(p)} h_a^p + \sum_{e \in \bigcup_{p \in P_a} \delta^+(p)} h_e^p \leq \mathcal{T} \sum_{i \in [N]} f_i^h(a) & \quad \forall a \in A \quad (6) \\
h_a + \sum_{p: a \in \delta^+(p)} h_a^p \geq r_a \sum_{i \in [N]} f_i^h(a) & \quad \forall a \in A \quad (7) \\
\sum_{a \in A} (\min\{c_{s(i)}^h, c_{s(a)}^h, \min_{\tilde{a} \in P_{s(a)}} c_{s(\tilde{a})}^h\} \cdot r_a + c_a^m) f_i^h(a) \leq R_i d_i & \quad \forall v \in \mathcal{R} \quad (8) \\
\sum_{a \in \delta^+(v)} t_a^p \leq \sum_{i \in [N]} f_i^h(a^*) & \quad \forall v \in V \ \forall p \in P^v \ \forall a^* \in p \quad (9) \\
\sum_{p: a \in \delta^+(p)} t_a^p \leq \sum_{i \in [N]} f_i^h(a) & \quad \forall a \in A \quad (10)
\end{aligned}$$

$$
\begin{aligned}
h_a^p &\leq \hat{\mathcal{T}}^p t_a^p && \forall p \in P^{ex}\ \forall a \in \delta^+(p) && (11)\\
f_i^\omega(A') &\in \mathbb{R}_{\geq 0} && \forall i \in [N]\ \forall \omega \in \{h,k\}\ \forall A' \in \mathcal{P}(A) &&\\
h_a^p &\in \mathbb{R}_{\geq 0} && \forall p \in P^{ex}\ \forall a \in \delta^+(p) &&\\
t_a^p &\in \mathbb{Z}_{\geq 0} && \forall p \in P^{ex}\ \forall a \in \delta^+(p) &&\\
h_a &\in \mathbb{R}_{\geq 0} && \forall a \in A. &&
\end{aligned}
$$

3 Labeling Algorithm

The main computational challenge of the HANP in Section 2 arises from the large number of variables, which severely affects tractability. In the literature, this issue is commonly addressed using a column generation framework, where the pricing problem is solved via a labeling algorithm. However, due to the complexity of our resource constraints, the pricing problem becomes particularly difficult to solve. For this reason, we adopt a labeling algorithm that directly solves the entire problem in a unified manner and which is designed to restrict computations to the information strictly necessary for identifying an optimal solution, thereby reducing the effective problem size.

Furthermore, conventional column generation techniques are not directly applicable to our formulation: Column generation typically benefits from a path-based form that allows the generation of variables corresponding to feasible paths. Although the solution for each commodity can indeed be represented as a set of feasible paths, the hydrogen-specific constraints—most notably the possibility of transferring transport capacity between vertices—render a standard path-based multicommodity flow formulation inadequate. Consequently, an arc-based formulation becomes necessary. However, this comes at the cost of introducing a large number of variables, many of which are irrelevant for determining an optimal solution. To overcome this limitation while exploiting the path-based interpretability of the solution, the proposed labeling algorithm efficiently incorporates the hydrogen-specific constraints into a dynamic programming labeling algorithm. It iteratively constructs and extends feasible path fragments through labels, explicitly accounting for the transfer and availability of transport capacity across the network.

The algorithm consists of several interconnected subprocedures, collectively forming the Hydrogen Aviation Network Labeling Algorithm (HANLA). We begin with a high-level overview of the full method before detailing each subprocedure. To this end, let $G = (V, A)$ be the directed graph introduced in Section 2, together with the associated notation. Denote by $\mathcal{W} \subseteq A$ the set of arcs that have already been labeled, and by $\mathcal{X} \subseteq V$ the set of vertices with positive hydrogen capacity, i.e., $\mathcal{H}_v > 0$. Let $\mathcal{L}$ denote a set of postponed vertex labels, as further described in Sect. 3.1.3. For each arc $a \in A$, define the hydrogen operating cost per passenger

$$
c_a^h := c_v^h \cdot r_a + c_a^m, \tag{12}
$$

where v is the source of a, c_v^h the hydrogen cost at v and c_a^m the non-fuel direct operating cost (non-fuel DOC) to operate arc a. Note that the correctness of the algorithm requires the triangle inequality to hold for the arc lengths in the network. Let $s(p)$ and $t(p)$ denote the source and target of a path p, respectively, and for each arc $a \in A$, let $s(a)$ and $t(a)$ denote its source and target. The structure of the HANLA is outlined in Algorithm 1.

HANLA computes a cost-minimal, demand-fulfilling flow in a directed graph. The algorithm begins by computing transport capacities as defined in Definition 2.1 and initializes with a feasible solution. It proceeds by iteratively applying a labeling procedure, starting from the arc with the lowest hydrogen cost to operate an arc, to construct feasible paths that satisfy the demand. Airports that deplete their hydrogen capacity are removed from the active set $\mathcal{X}$, and labeled arcs are recorded in $\mathcal{W}$. In each iteration, the next arc is selected based on minimal cost and the presence of unlabeled outgoing arcs. The main loop terminates when all arcs have been labeled or no available hydrogen remains. In a subsequent post-processing step, any postponed vertex labels in $\mathcal{L}$ are revisited and evaluated, ensuring that all feasible label extensions are considered and yielding a cost-optimal flow assignment.

3.1 Labels and Subprocedures

To introduce the subprocedures, it is necessary to define the different labels used within the algorithm: the arc labels, defined for individual arcs and used to reconstruct a full solution, and the vertex labels, maintained per vertex and encoding entire feasible paths that may not yet be optimal but represent feasible components of the final solution.

Algorithm 1: Hydrogen Aviation Network Labeling Algorithm (HANLA)

Input: $G = (V, A)$, c_a^h hydrogen cost for all $a \in A$, $\mathcal{H}_v$ hydrogen capacity for all $v \in V$
Output: cost-minimal, demand-fulfilling flow per commodity

1 Precomputation Transport Capacity(G) `// Algorithm 2`
2 Initialization(G) `// Algorithm 3`
3 $\mathcal{W} \leftarrow \emptyset$, $\mathcal{X} \leftarrow V \setminus \{v : \mathcal{H}_v = 0\}$, $\mathcal{L} \leftarrow \emptyset$
4 $y \leftarrow \text{argmin}\{c_a^h : a \in A\}$, $y =: (u, v)$
5 **while** $\mathcal{W} \neq A$ **and** $\mathcal{X} \neq \emptyset$ **do**
6   Labeling(y) `// Algorithm 4`
7   **if** $\mathcal{H}_u = 0$ **then**
8         $\mathcal{X} \leftarrow \mathcal{X} \setminus \{u\}$
9     $\mathcal{W} \leftarrow \mathcal{W} \cup \{y\}$
10   **if** $(v, u) \in A$ **and** $(v, u) \notin \mathcal{W}$ **then**
11         $y \leftarrow (v, u)$
12   **goto line 6**
13     $y \leftarrow \text{argmin}\{c_a^h : \textbf{if } A \setminus \mathcal{W} \cap \delta^+(v) \neq \emptyset \textbf{ then } a \in A \setminus \mathcal{W} \cap \delta^+(v) \textbf{ else } a \in A \setminus \mathcal{W}\}$
14 **for** $\vartheta \in \mathcal{L}$ **do**
15   Arc Labeling(ϑ) `// Algorithm 5`

Definition 3.1 (Vertex Label)**.** *A* ***vertex label*** *is a label $\vartheta_v = [\gamma, \eta, \zeta, \varpi]$ at vertex $v \in V$. Let $\mathcal{V}$ be the set of vertex labels, $\mathcal{V}_v^+$ be the set of vertex labels with paths starting and $\mathcal{V}_v^-$ be the set of vertex labels with path ending in a specific vertex $v \in V$.*

Each vertex label represents a feasible path for a commodity that either originates or terminates at the vertex associated with the label. Note that $\bigcup_{v \in V} \mathcal{V}_v^- = \mathcal{V}$ and $\bigcup_{v \in V} \mathcal{V}_v^+ = \mathcal{V}$, i.e., every vertex label appears in both sets. This property is essential for the labeling procedure described in Sect. 3.1.3.

In Definition 3.1, let $\gamma(\vartheta_v) = \gamma \in \mathbb{R}$ denote the cost of operating the path $\zeta(\vartheta_v) = \zeta \in \mathcal{P}(A)$ for a single passenger and let $\varpi \in \{k, h, t^p\}^\zeta$ be the power mode for every arc within ζ. Furthermore, we associate with each label the variable $\eta(\vartheta_v) = \eta \in \mathbb{R}$, representing the amount of unused transport capacity along the path. Note that within the path ζ, hydrogen can be supplied at each arc's source vertex via an independent hydrogen excess path. The value η indicates whether the transport capacity is fully utilized or if surplus capacity remains.

Now we define some variables needed for the arc label $\epsilon_{a,i,\vartheta}^\beta$ for arc $a \in A$, commodity $i \in [N]$, power mode $\beta \in \{k, h, t^p\}$ and vertex label $\vartheta \in \mathcal{V}$. The vertex label gives the associated path and ensures that each arc label is uniquely defined. The arc labels will be of the form $\epsilon_{a,i,\vartheta}^\beta = [\nu, \rho, \sigma, \xi, \phi, \psi, \chi]$, where $\nu(\epsilon_{a,i,\vartheta}^\beta) = \nu \in \mathbb{N}$ represents the part of the demand of commodity i that is covered by this label, $\rho(\epsilon_{a,i,\vartheta}^\beta) = \rho \in \mathbb{R}$ denotes the costs for the whole path operated for one passenger and $\sigma(\epsilon_{a,i,\vartheta}^\beta) = \sigma \in A$ the previous arc in the path to reproduce the whole path used. For that, $\xi(\epsilon_{a,i,\vartheta}^\beta) = \xi \in \{h, k, t^p\}$ also indicates whether the previous arc is operated by hydrogen (h), kerosene (k) or transport capacity (t^p). As we need to maintain a record whether the hydrogen capacity at each airport is met, we also need to observe of how much of the hydrogen used to operate a is bought at the source of a, indicated via $\phi(\epsilon_{a,i,\vartheta}^\beta) = \phi \in \mathbb{R}$, and how much is bought at another source via a transport capacity, indicated by $\psi(\epsilon_{a,i,\vartheta}^\beta) = \psi \in \mathbb{R}$. For the latter we also need to know where the hydrogen comes from, indicated by $\chi(\epsilon_{a,i,\vartheta}^\beta) = \chi \subseteq V$, where χ is a hydrogen excess path.

Definition 3.2 (Arc Label)**.** *Let $\epsilon_{a,i,\vartheta}^\beta = [\nu, \rho, \sigma, \xi, \phi, \psi, \chi]$ be a label for arc $a \in A$, commodity $i \in [N]$, $\beta \in \{k, h, t^p\}$ and vertex label $\vartheta \in \mathcal{V}$. Let $\mathcal{E}$ be the set of arc labels and let $\mathcal{E}_i$ be the set of all arc labels for arcs ending a path for commodity i. If*

$$\sum_{\epsilon_{a,i,\vartheta}^\beta \in \mathcal{E}_i} \nu(\epsilon_{a,i,\vartheta}^\beta) = Qd_i \qquad \forall i \in [N] \tag{13}$$

$$\nu(\epsilon_{a,i,\vartheta}^\beta) = \nu(\epsilon_{\sigma(\epsilon_{a,i,\vartheta}^\beta),i,\vartheta}^{\xi(\epsilon_{a,i,\vartheta}^\beta)}) \qquad \forall \epsilon_{a,i,\vartheta}^\beta \in \mathcal{E}\ \forall i \in [N] \tag{14}$$

$$\rho(\epsilon^{\beta}_{a,i,\vartheta}) = \rho(\epsilon^{\xi(\epsilon^{\beta}_{a,i,\vartheta})}_{\sigma(\epsilon^{\beta}_{a,i,\vartheta}),i,\vartheta}) \qquad \forall \epsilon^{\beta}_{a,i,\vartheta} \in \mathcal{E} \ \forall i \in [N] \tag{15}$$

holds, we call $\epsilon^{\beta}_{a,i,\vartheta}$ an ***arc label****.*

(13) ensures that in each step of our algorithm the total demand of each commodity is satisfied. Here we also consider the market penetration Q: The hydrogen powered flow is constrained by Q, while kerosene powered flow has no capacity restriction. Consequently, the part of the demand larger than Qd_i can and must be kerosene powered. Hence, we can fix the solution for this part of the demand as a preprocessing step and do not need to consider it in our algorithm. For better readability, we will omit Q in the following and d_i denotes the demand restricted by Q. Furthermore, in (14) and (15) we make sure that the demand and cost information of each arc label belonging to the same path are equal.

Note that an arc can have multiple labels for one commodity.

3.1.1 Precomputation of Transport Capacity

Hydrogen excess paths, as defined in Definition 2.1, and their respective transport capacities are required for the HANLA, and will be computed prior to the execution of the actual labeling.

Lemma 3.3. *To compute the hydrogen excess paths we only need to consider the path which maximizes the transport capacity for each pair of vertices $(o, u) \in V \times V$.*

Proof. Let $i \in [N]$ denote an arbitrary commodity, and let $o \in V$ and $u \in V$ be its associated origin and destination, respectively. Among all possible hydrogen excess paths from o to u, the one that yields the highest transport capacity at u is the path that minimizes the total hydrogen consumption. In other words, the path with the maximum transport capacity is the shortest path from o to u with respect to hydrogen consumption. This follows directly from the definition of the transport capacity $\hat{\mathcal{T}}^p$ of a hydrogen excess path p, given by

$$\hat{\mathcal{T}}^p = \mathcal{T} - \sum_{j=1}^{M} r_j, \tag{16}$$

where r_j denotes the hydrogen consumption of the j-th arc in path p, and M is the number of arcs in p. Minimizing the sum $\sum_{j=1}^{M} r_j$ thus maximizes $\hat{\mathcal{T}}^p$.

Ignoring hydrogen supply constraints, this shortest path represents the optimal strategy for serving the demand of commodity i using hydrogen. If this path cannot be operated exclusively with hydrogen sourced from o, then no other path from o to u would be able to do so either, since any alternative path would have a higher total hydrogen consumption and therefore a lower transport capacity.

It follows that transport capacity from o to u can be utilized only if sufficient hydrogen to operate the entire shortest hydrogen excess path exclusively using hydrogen from the origin is available at o. Thus, it is sufficient to only compute the hydrogen excess paths with the highest transport capacity. □

Let Q_v denote the set of shortest paths wrt. r from $v \in V$ to all other vertices and $Q_v[u]$ the shortest path from v to u. Let D_v be the distance matrix, where $D_v[u]$ represents the length of the shortest path from v to u contained in Q_v. The sets Q_v and matrices D_v can be obtained, for instance, by applying Dijkstra's algorithm to each vertex $v \in V$. The hydrogen excess paths are then computed as described in Algorithm 2.

3.1.2 Initialization

The second step in the HANLA is the initialization of the algorithm with a feasible solution, the corresponding procedure is described in Algorithm 3.

For each commodity $[v, u]$, we proceed as follows. If a direct arc (v, u) exists, we check whether it can be operated entirely using hydrogen. If so, the arc is assigned to hydrogen operation; otherwise, it is operated with kerosene. If no direct arc exists, the commodity is routed along a shortest v–u path (with respect to kerosene costs) and operated with kerosene. We denote by $\varsigma_{[v,u]}$ the resulting cost bound for commodity $[v, u]$, which will be used in Algorithm 4.

This solution is in fact feasible for HANP, as shown in Theorem 3.4. Let $\mathcal{E}^h$ be the set of arc labels for hydrogen powered flow and let $\mathcal{E}^k$ be the set of arc labels regarding kerosene powered flow.

Algorithm 2: Precomputation of Transport Capacity

Input: transportable hydrogen per passenger $\mathcal{T}$, hydrogen consumption r_a per passenger for all arcs $a \in A$, Q_v set of shortest paths wrt. r_a, D_v distance matrix for all $v \in V$

Output: set P^{ex} of all possible hydrogen excess paths p with their respective transport capacity $\hat{\mathcal{T}}_v^p$ for their starting vertex $v \in V$

Procedure Precomputation Transport Capacity*(G)*:
- $P^{ex} \leftarrow \emptyset$
- **for** $v \in V$ **do**
  - **for** $u \in V$ **do**
    - **if** $D_v[u] < \mathcal{T}$ **then**
      - $P^{ex} \leftarrow P^{ex} \cup \{Q_v[u]\}$
      - $\hat{\mathcal{T}}_v^{Q_v[u]} \leftarrow \mathcal{T} - D_v[u]$

Algorithm 3: Initial Feasible Solution

Input: hydrogen consumption r_a per passenger, cost c_a^h and c_a^k for all $a \in A$, hydrogen capacity $\mathcal{H}_v$ for all $v \in V$, transportable hydrogen per passenger $\mathcal{T}$, demand d_i for all commodities $i \in [N]$

Output: feasible solution to HANP given in arc and vertex labels, cost bound ς_i per commodity $i \in [N]$

Procedure Initialization*(G)*:
- **for** $v \in V$ **do**
  - **for** $u \in V \setminus \{v\}$ **do**
    - $i \leftarrow [v, u]$
    - **if** $a = (v, u) \in A$ **then**
      - **if** $\sum_{\tilde{a} \in \delta^+(v)} r_{\tilde{a}} d_{[v,t(\tilde{a})]} \leq \mathcal{H}_v \ \wedge\ c_a^h < c_a^k \ \wedge\ r_a < \mathcal{T}$ **then**
        - $\varsigma_{[v,u]} \leftarrow c_a^h$
        - $\vartheta_v \leftarrow [c_a^h, 0, \{(v, u)\}, (h)]$
        - $\epsilon^h_{a,i,\vartheta_v} \leftarrow [d_i, c_a^h, -1, -1, r_a d_i, 0, \emptyset]$
        - $\mathcal{H}_v \leftarrow \mathcal{H}_v - r_a d_i$
      - **else**
        - $\varsigma_{[v,u]} \leftarrow c_a^k$
        - $\vartheta_v \leftarrow [c_a^k, 0, \{(v, u)\}, (k)]$
        - $\epsilon^k_{a,i,\vartheta_v} \leftarrow [d_i, c_a^k, -1, -1, 0, 0, \emptyset]$
    - **else**
      - Let $(a_1, \ldots, a_m)$ be the shortest path from v to u wrt. c_a^k
      - $\varsigma_{[v,u]} \leftarrow \sum_{z=1}^m c^k_{a_z}$
      - $\vartheta_v \leftarrow [\sum_{z=1}^m c^k_{a_z}, 0, (a_1, \ldots, a_m), (k, \ldots, k)]$
      - **for** $a_j \in \{a_1, \ldots, a_m\}$ **do**
        - $\epsilon^k_{a_j,i,\vartheta_v} \leftarrow [d_i, \varsigma_{[v,u]}, a_{j-1}, k, 0, 0, \emptyset]$; `// with` $a_0 := -1$

Theorem 3.4. *A feasible solution to the Hydrogen Aviation Network Problem (HANP) can be defined as follows: for each commodity i and arc $a \in A$, let*

$$f_i^h(a) = \begin{cases} \nu(\epsilon_{a,i,\vartheta}^h), & \text{if } \epsilon_{a,i,\vartheta}^h \in \mathcal{E}^h, \\ 0, & \text{otherwise}, \end{cases}, \qquad f_i^k(a) = \begin{cases} \nu(\epsilon_{a,i,\vartheta}^k), & \text{if } \epsilon_{a,i,\vartheta}^k \in \mathcal{E}^k, \\ 0, & \text{otherwise}, \end{cases}$$

with $\mathcal{E}^h$ and $\mathcal{E}^k$ calculated in Algorithm 3. Furthermore, for each arc $a \in A$, set

$$h_a = r_a\, f_i^h(a), \tag{17}$$

and initialize $h_a^p = 0$ and $t_a^p = 0$ for all hydrogen excess paths $p \in P^{ex}$ and arcs $a \in A$.

Proof. The feasibility of the solution can be easily seen by inserting all the values into the model for HANP defined in Section 2. Note that the flow values are well-defined since there is only one arc label per arc as the solution either uses hydrogen or kerosene-powered operation for an arc, so (1) to (4) hold. (5) holds because of line 6 in Algorithm 3. No transport capacity is used, so inequalities (6) to (7) reduce to a direct comparison in the form of (17), and (9) to (11) reduce to non-negativity conditions on the flow variables. □

3.1.3 Labeling

The final subprocedure is the labeling routine within the main loop of HANLA. As shown in Algorithm 1, this loop iterates over all arcs $y = (u, v) \in A$ or terminates when no vertex with remaining hydrogen capacity remains. The labeling procedure comprises three main parts, each using the current arc y to generate new paths and labels. These parts differ in how y is combined with the paths of existing vertex labels. In *forward labeling (FL)*, labels from $\mathcal{V}_u^-$ are extended by appending arc y to the end of their path. In *backward labeling (BL)*, labels from $\mathcal{V}_v^+$ are extended by prepending y to the start of their path. A third option considers y as a path on its own. Let κ be the resulting path. Let $\vartheta = [\gamma, \eta, \zeta, \varpi]$ denote the vertex label with either $\vartheta \in \mathcal{V}_u^-$ in case of FL or $\vartheta \in \mathcal{V}_v^+$ in case of BL. In case of y on its own, the costs γ and unused transport capacity η are set to 0 and the path ζ is the empty path. Once candidate paths are constructed, the algorithm checks whether they offer a cost improvement. At this point, the operation mode of arc y—kerosene, hydrogen, or transported hydrogen—is not yet fixed.

Let $\beta \in \{k, h, t^p\}$ (kerosene, hydrogen, or transported hydrogen by path p) be the chosen power mode for an arc a. Note that in case of t^p, if the transport capacity is not enough to serve the upcoming arc alone, refueling with the missing hydrogen at the starting airport of the arc is possible. Let $c_a^{t^p}$ be the cost to operate arc a with transport capacity $\hat{\mathcal{T}}^p$ coming from the hydrogen excess path p. In case $r_a > \hat{\mathcal{T}}^p$, the cost comprises both the cost for the transported hydrogen and the cost for the hydrogen that needs to be refueled at the source of a. Each mode has different implications for cost and capacity.

Let q and w denote the start and end point of κ, respectively, and let $\varsigma_{[q,w]}$ be the cost bound to transport the commodity from q to w, set to the cost of the initial solution retrieved in Algorithm 3. κ is a cost-improving path if

$$c_y^\beta + \gamma < \varsigma_{[q,w]} \tag{18}$$

for one $\beta \in \{k, h, t^p\}$ holds. If $r_y > \mathcal{T}$, we assume that the cost c_y^β is infinite for modes $\beta \in \{h, t^p\}$ due to refueling limits.

If condition (18) holds, new vertex labels $\tilde{\vartheta} = [\tilde{\gamma}, \tilde{\eta}, \kappa, \tilde{\varpi}]$ are placed at the start and end nodes of κ, with total cost $\tilde{\gamma} = \gamma + c_y^\beta$, $(\tilde{\varpi}_a)_{a\in\zeta} = (\varpi_a)_{a\in\zeta}$, and $\tilde{\varpi}_y = \beta$. For kerosene or hydrogen modes, $\tilde{\eta} = \eta$ from the parent vertex label ϑ. For transported hydrogen, if the whole transport capacity is used, $\tilde{\eta} = 0$, otherwise the unused portion is recorded in $\tilde{\eta}$. Such partial-use labels are only considered in the final phase of HANLA when updating arc labels. Let $\mathcal{L}$ denote this set of postponed labels, which must be sorted non-decreasingly with respect to η. This is crucial for the optimality of the labeling algorithm as using a higher amount of a certain transport capacity – represented by lower η-value – results in a higher cost saving within the overall model. This procedure is summarized in Algorithm 4.

Next, κ is evaluated for improving arc labels. For all arc labels $\epsilon_{a,i,\vartheta}^\beta = \epsilon \in \mathcal{E}$ with $i = [q, w]$, we check if $\tilde{\gamma} \le \rho(\epsilon)$ holds. Let D denote the portion of passenger demand that could be served at a cheaper price via κ, i.e., $D \coloneqq \sum_{\epsilon:\tilde{\gamma}\le\rho(\epsilon)} \nu(\epsilon)$.

To determine how much demand κ can feasibly carry, capacity constraints must be respected for hydrogen-powered arcs. Let $a_\ell \in A$ with $\ell \in [L]$ be the hydrogen-operated arcs in κ. For each a_ℓ, let $\mathcal{Q}_\ell$

Algorithm 4: Labeling

Input: arc $y = (u, v)$ to be labeled, costs c_y^k, c_y^h, $c_y^{t^p}$, cost bound ς_i for all commodities $i \in [N]$, hydrogen consumption r_y

Output: new vertex and arc labels

Procedure Labeling*(y)*:
  for $\vartheta = [\gamma, \eta, \zeta, \varpi] \in \mathcal{V}_u^-$ **do**
    Path Labeling(ϑ, (ζ, y), y) `// Forward Labeling`
  for $\vartheta = [\gamma, \eta, \zeta, \varpi] \in \mathcal{V}_v^+$ **do**
    Path Labeling(ϑ, (y, ζ), y) `// Backward Labeling`
  Path Labeling($[0, 0, \emptyset, ()]$, (y), y)

Procedure Path Labeling*(ϑ, κ, y)*:
  $q \leftarrow s(\kappa)$, $w \leftarrow t(\kappa)$
  for $\beta \in \{k, h, t^p\}$ **do**
    if $c_y^\beta + \gamma < \varsigma_{[q,w]}$ **then**
      if $\beta \in \{k, h\}$ **then** $\tilde{\eta} \leftarrow \eta$
      else if $\beta = t^p$ **then**
        $\mathcal{T}^p \leftarrow$ transport capacity serving y
        if $\mathcal{T}^p < r_y$ **then** $\tilde{\eta} \leftarrow 0$
        else $\tilde{\eta} \leftarrow \min\{\eta, \mathcal{T}^p - r_y\}$
      $\tilde{\varpi}_y \leftarrow \beta$, $(\tilde{\varpi}_a)_{a \in \zeta} \leftarrow (\varpi_a)_{a \in \zeta}$
      $\tilde{\vartheta} \leftarrow [c_y^\beta + \gamma, \tilde{\eta}, \kappa, \tilde{\varpi}]$
      $\mathcal{V}_q^+ \leftarrow \mathcal{V}_q^+ \cup \{\tilde{\vartheta}\}$, $\mathcal{V}_w^- \leftarrow \mathcal{V}_w^- \cup \{\tilde{\vartheta}\}$ `// new vertex labels`
      if $\tilde{\eta} \neq 0 \lor ((\tilde{\varpi}_a)_{a \in \zeta} = t^p \land$ some arc in p not labeled yet*)* **then**
        $\mathcal{L} \leftarrow \mathcal{L} \cup \{\tilde{\vartheta}\}$
      else
        Arc Labeling($\tilde{\vartheta}$, $[q, w]$) `// Algorithm 5`

be the amount of passenger demand that can be served by the available hydrogen at its source, and let $\mathcal{Q}_\ell^t$ be the passenger demand that can be served by the hydrogen available via transport capacity, if used. If no transport capacity is involved, $\mathcal{Q}_\ell^t = 0$. To avoid infeasible empty flights, transported hydrogen must coincide with actual passenger flow. Let $p_\ell = (e_1, \dots, e_{J_\ell})$ be the hydrogen excess path supporting transported hydrogen on arc a_ℓ and let Δ_j be the passenger flow on arc e_j, $j \in [J_\ell]$, so that (10) will be fulfilled. If no transport capacity is used, p_ℓ is empty, thus Δ not present in the minimum in (19). Then, the maximum feasible passenger demand that κ can serve is

$$\mathcal{D} \coloneqq \max\{\min\{D, \mathcal{Q}_\ell : \ell \in [L]\}, \min\{D, \mathcal{Q}_\ell + \mathcal{Q}_\ell^t, \Delta_j : \ell \in [L],\ j \in [J_\ell]\}\}. \tag{19}$$

Note that when transport capacity is utilized, intermediate refueling at the source vertex of an arc is permitted if the available hydrogen from the transport capacity is insufficient to operate the entire arc using the hydrogen from the transport capacity. The value $\mathcal{D}$ is then used to update the arc labels for κ, thereby capturing both improved cost efficiency and feasible capacity usage.

Let $\mathcal{E}_i$ be the subset of $\mathcal{E}$ with arc labels $\epsilon_{a,i,\vartheta}^{\beta}$ for arcs ending a path for commodity i. This set is sorted in non-decreasing order with respect to the costs ρ, ensuring that arc labels with higher cost are processed first to achieve maximal potential cost savings. This ordering is essential for the optimality of the algorithm: Since costs are commodity-independent and the labeling procedure follows a specified order, all relevant lower-cost arcs have already been labeled when a vertex label is considered for the current feasible solution. Consequently, once a vertex label is included in the current feasible solution, it is never necessary to replace it with a higher-cost alternative at a later stage, which preserves optimality at the end of the algorithm. The algorithmic steps are presented in Algorithm 5.

3.2 Correctness and Optimality of HANLA

This subsection establishes the feasibility of solutions obtained via Algorithm 1 and culminates in proving that HANLA computes a correct and optimal solution. We begin by showing that the labels assigned to arcs by HANLA are valid arc labels.

Lemma 3.5. *During Algorithm 4, every element in the set $\mathcal{E}$ is an arc label, i.e., the equations defined in Definition 3.2 are fulfilled at every iteration of HANLA.*

Proof. We first show that the arc labels in the initial set $\mathcal{E}$, constructed in Algorithm 3, satisfy the equations stated in Definition 3.2. For each commodity, exactly one flow satisfying its full demand is selected. Consequently, (13) holds trivially. Moreover, for every arc on the corresponding path, the associated labels are initialized with identical data. Thus, the consistency conditions eqs. (14) and (15) are satisfied for all labels created during initialization.

We now examine how the set $\mathcal{E}$ is modified during the main loop of HANLA. Arc labels are altered exclusively within Algorithm 5, where labels may be deleted and newly assigned. In the first for-loop in line 5, all labels corresponding to an entire path of the current solution are removed. Following this deletion step, (13) is no longer satisfied, but eqs. (14) and (15) hold for the remaining label. In the second for-loop, starting in line 32, new labels are introduced along a new path, carrying exactly the same amount E of demand as the deleted flow. These labels are assigned consistently for every arc of the newly selected path, ensuring that (14) and (15) hold. Since the amount of demand introduced equals the amount removed, (13) is restored. Therefore, after each execution of the Arc Labeling procedure, all inequalities from Definition 3.2 continue to hold. □

We now show how to construct a feasible solution for HANP from an arc label set $\mathcal{E}$. For readability let $\mathcal{V}(a, i, \beta) \coloneqq \{\vartheta : \epsilon_{a,i,\vartheta}^{\beta} \text{ exists}\}$.

Lemma 3.6. *Let $\mathcal{E}$ be the set of arc labels obtained at an arbitrary iteration of HANLA. A feasible solution of the HANP can be constructed from $\mathcal{E}$ as follows:*

$$f_i^k(a) \coloneqq \sum_{\vartheta \in \mathcal{V}(a,i,\beta)} \nu(\epsilon_{a,i,\vartheta}^{k}) \qquad \forall i \in [N]\ \forall a \in A$$

$$f_i^h(a) \coloneqq \sum_{\substack{\beta \in \{h, t^p\} \\ \vartheta \in \mathcal{V}(a,i,\beta)}} \nu(\epsilon_{a,i,\vartheta}^{\beta}) \qquad \forall i \in [N]\ \forall a \in A$$

Algorithm 5: Arc Labeling

Input: vertex label $\tilde{\vartheta}$ giving the new path, hydrogen capacity $\mathcal{H}_v$ for all $v \in V$
Output: updated arc labels

Procedure Arc Labeling*($\tilde{\vartheta}$, $i = [q, w]$)***:**
  $\mathcal{D} \leftarrow \max\{\min\{D, \mathcal{Q}_\ell : \ell \in [L]\},\ \min\{D, \mathcal{Q}_\ell + \mathcal{Q}^t_\ell, \Delta_j : \ell \in [L],\ j \in [J_\ell]\}\}$ `// def. in` (19)
  $E \leftarrow 0$
  $\mathcal{E}_i \leftarrow$ list of arc labels both associated with i and arcs belonging to $\delta^-(w)$, ordered non-decreasingly wrt. cost
  `// remove old arc labels`
  for $\epsilon^\beta_{a,i,\vartheta} = \epsilon \in \mathcal{E}_i$ **do**
    if $\gamma(\tilde{\vartheta}) < \rho(\epsilon)$ **and** $E < \mathcal{D}$ **then**
      if $E + \nu(\epsilon) < \mathcal{D}$ **then**
        $\mathcal{E}_i \leftarrow \mathcal{E}_i \setminus \epsilon$
        $E \leftarrow E + \nu(\epsilon)$
        do
          $\mathcal{H}_{s(a)} \leftarrow \mathcal{H}_{s(a)} + \phi(\epsilon)$
          $\mathcal{H}_{s(\chi(\epsilon))} \leftarrow \mathcal{H}_{s(\chi(\epsilon))} + \psi(\epsilon)$
          $\mathcal{E} \leftarrow \mathcal{E} \setminus \epsilon$
          $\tilde{\epsilon} \leftarrow \epsilon,\ \ \epsilon \leftarrow \epsilon^{\xi(\epsilon)}_{\sigma(\epsilon),i,\vartheta}$
        while $\sigma(\tilde{\epsilon}) \neq -1$
      else
        do
          if $\beta = t^p$ **then**
            if $\mathcal{T}^p \leq r_a$ **then** $\tilde{\phi} = (r_a - \mathcal{T}^p)(\mathcal{D} - E),\ \ \tilde{\psi} = \mathcal{T}^p(\mathcal{D} - E)$
            else $\tilde{\phi} = 0,\ \ \tilde{\psi} = \mathcal{T}^p(\mathcal{D} - E)$
          else if $\beta = h$ **then**
            $\tilde{\phi} = r_a(\mathcal{D} - E),\ \ \tilde{\psi} = 0$
          $\nu(\epsilon) \leftarrow \nu(\epsilon) - (\mathcal{D} - E)$
          $\phi(\epsilon) \leftarrow \phi(\epsilon) - \tilde{\phi}$
          $\psi(\epsilon) \leftarrow \psi(\epsilon) - \tilde{\psi}$
          $\mathcal{H}_{s(a)} \leftarrow \mathcal{H}_{s(a)} + \tilde{\phi}$
          $\mathcal{H}_{s(\chi(\epsilon))} \leftarrow \mathcal{H}_{s(\chi(\epsilon))} + \tilde{\psi}$
          $\tilde{\epsilon} \leftarrow \epsilon,\ \ \epsilon \leftarrow \epsilon^{\xi(\epsilon)}_{\sigma(\epsilon),i,\vartheta}$
        while $\sigma(\tilde{\epsilon}) \neq -1$
        $E \leftarrow \mathcal{D}$
  `// add new arc labels`
  if $E > 0$ **then**
    for $e_f \in \zeta(\tilde{\vartheta}) = (e_1, ..., e_F)$ **do**
      if $\varpi_{e_f}(\tilde{\vartheta}) = t^p$ **then**
        $p \leftarrow$ hydrogen excess path serving e_f, $\ \mathcal{T}^p \leftarrow$ associated transport capacity.
        if $\mathcal{T}^p \leq r_{e_f}$ **then** `// with` $e_0 := -1$, $\varpi_{e_0}(\tilde{\vartheta}) := -1$
          $\mathcal{E} \leftarrow \mathcal{E} \cup [E, \gamma(\tilde{\vartheta}), e_{f-1}, \varpi_{e_{f-1}}(\tilde{\vartheta}), E(r_{e_f} - \mathcal{T}^p), E\mathcal{T}^p, p]$
          $\mathcal{H}_{s(e_f)} \leftarrow \mathcal{H}_{s(e_f)} - E(r_{e_f} - \mathcal{T}^p)$
          $\mathcal{H}_{s(p)} \leftarrow \mathcal{H}_{s(p)} - E\mathcal{T}^p$
        else
          $\mathcal{E} \leftarrow \mathcal{E} \cup [E,\ \gamma(\tilde{\vartheta}),\ e_{f-1},\ \varpi_{e_{f-1}}(\tilde{\vartheta}),\ 0,\ Er_{e_f},\ p]$
          $\mathcal{H}_{s(p)} \leftarrow \mathcal{H}_{s(p)} - E\mathcal{T}^p$
      else if $\varpi_{e_f}(\tilde{\vartheta}) = h$ **then**
        $\mathcal{E} \leftarrow \mathcal{E} \cup [E,\ \gamma(\tilde{\vartheta}),\ e_{f-1},\ \varpi_{e_{f-1}}(\tilde{\vartheta}),\ Er_{e_f},\ 0,\ \emptyset]$
        $\mathcal{H}_{s(e_f)} \leftarrow \mathcal{H}_{s(e_f)} - Er_{e_f}$
      else if $\varpi_{e_f}(\tilde{\vartheta}) = k$ **then**
        $\mathcal{E} \leftarrow \mathcal{E} \cup [E,\ \gamma(\tilde{\vartheta}),\ e_{f-1},\ \varpi_{e_{f-1}}(\tilde{\vartheta}),\ 0,\ 0,\ \emptyset]$

$$h_a := \sum_{\substack{i\in[N]\\ \beta\in\{h,t^p\}\\ \vartheta\in\mathcal{V}(a,i,\beta)}} \phi(\epsilon^{\beta}_{a,i,\vartheta}) \qquad \forall a \in A$$

$$h^p_a := \sum_{\substack{i\in[N]\\ \vartheta\in\mathcal{V}(a,i,\beta)}} \psi(\epsilon^{t^p}_{a,i,\vartheta}) \qquad \forall p \in P^{ex}\ \forall a \in \delta^+(p)$$

$$t^p_a := \sum_{\substack{i\in[N]\\ \vartheta\in\mathcal{V}(a,i,\beta)}} \nu(\epsilon^{t^p}_{a,i,\vartheta}) \qquad \forall p \in P^{ex}\ \forall a \in \delta^+(p).$$

Proof. Lemma 3.5 shows that the labels in $\mathcal{E}$ fulfill the equations in Definition 3.2. The flow constraints (1) to (4) of our network are then met via the properties of the arc labels: (15) ensures that the demand of each commodity is fulfilled (eqs. (1) and (2)) and also incorporates the market penetration; (13) makes sure that the flow conversation is satisfied. Inequalities (5) and (7) are ensured by the definition of $\mathcal{Q}$ and $\mathcal{Q}^t$ in Algorithm 4. Inequality (6) limits the amount of portable hydrogen on a flight to a specific tank size and is ensured via excluding arcs from the labeling where $r_a > \mathcal{T}$ holds and via the definition of the transport capacity. (8) is fulfilled due to the definition of the cost bound of each commodity. Inequalities (9) and (10) make sure that there are no empty flights necessary to fulfill the flow in our network. In HANLA this is ensured via the definition of Δ in Algorithm 4. The transport capacity then also ensures inequality (11). $\square$

Finally, we prove that Algorithm 1 correctly computes an optimal solution.

Theorem 3.7. *The solution of the Hydrogen Aviation Network Labeling Algorithm, introduced in Algorithm 1, is optimal for the Hydrogen Aviation Network Problem, introduced in Section 2.*

Proof. Let $\mathcal{E}$ be the arc label set after termination of HANLA, and let x be the associated solution as shown in Lemma 3.6. Assume that there exists a solution $x^\star$ with lower objective function value than x. Then there exists a commodity i for which the total cost to operate the demand is lower for $x^\star$ than for x. As we consider purely homogeneous costs and no capacity restrictions for kerosene, shortest paths must be optimal for paths exclusively operated by kerosene, i.e., the initial solution is already optimal for these. Hence, within $x^\star$, there must exist a path $p^\star$ for commodity i with a higher usage of hydrogen than the utilized paths from x. Now, either there exists a vertex label for $p^\star$, but we did not consider it for the solution, or no vertex label exists for $p^\star$. Note that the only place where new vertex labels are set after the initialization is in line 18, Algorithm 4, and new arc labels following line 32, Algorithm 5.

Case 1: Assume that there exists a vertex label ϑ^* for $p^\star$, but that $p^\star$ is not used in x. Then $p^\star$ has strictly lower cost than the cost bound ς_i for commodity i (cf. line 10, Algorithm 4), yet no arc labels for ϑ^* exist. If these arc labels were created at some point but removed later on, this would mean that there must exist a better path than p^* in x. Hence, arc labels for ϑ^* were never created. This means that $E = 0$ in line 31 in Algorithm 5. Then either $\mathcal{D} = 0$ or E was never increased after its initialization. If $\mathcal{D} > 0$, but still $E = 0$, then $\gamma(\vartheta^*) \geq \rho(\epsilon)$ for all $\epsilon \in \mathcal{E}_i$. This means that p^* would indeed not be better than any path used for i. Therefore, $\mathcal{D} = 0 = \max\{\min\{D, \mathcal{Q}_\ell : \ell \in [L]\}, \min\{D, \mathcal{Q}_\ell + \mathcal{Q}^t_\ell, \Delta_j : \ell \in [L],\ j \in [J_\ell]\}\}$. By definition of D, if $D = 0$, then no passenger demand can be served cheaper by p^*. Thus, at least one of the values $\mathcal{Q}_\ell$, $\mathcal{Q}^t_\ell$ or Δ_j must be 0, meaning that one of the hydrogen operated arcs $a_\ell \in p^*$ does not have enough hydrogen available. Without loss of generality, assume that the violation occurs for a single arc $a_\ell = (u, v) \in A$. Note that different power modes on a_ℓ induce different capacity constraints, whereas kerosene operation is unconstrained and does not need consideration.

Case 1a: $\varpi_{a_\ell}(\vartheta) = h$ and $\mathcal{Q}_\ell = 0$ holds, and thus, the hydrogen capacity at u is exhausted. Redistributing hydrogen to enable usage of p^* cannot yield a strict improvement: Since costs are commodity-independent and because of the specified ordering of the labeling, all relevant cheaper arcs have already been labeled, i.e., pulling hydrogen from a previously labeled path p must lead to using a path p' instead of p that is more expensive than $p^\star$. Hence, $p^\star$ cannot strictly improve x.

Case 1b: $\varpi_{a_\ell}(\vartheta) = t^p$, then arc a_ℓ is operated using transport capacity induced by a hydrogen excess path p from some $\tilde{u}$ to u. If $\mathcal{Q}^t_\ell = 0$, i.e., the hydrogen capacity at $\tilde{u}$ is exhausted, the argument from the previous case applies. Hence, $\Delta_j = 0$ for one arc $\tilde{a}_j \in p$. All arcs of p must be labeled unless the algorithm terminates early due to $\mathcal{H}_v = 0$ for all $v \in V$: vertex labels that depend on arcs of p that are not yet labeled are deferred to the final stage of the algorithm (cf. line 19 in Algorithm 5). Consequently, upon consideration of such labels, all arcs of p have been labeled (cf. line 15 in Algorithm 1). *Case 1b.i:* If the algorithm terminates early due to $\mathcal{H}_v = 0$ for all $v \in V$, then no hydrogen remains available to operate $\tilde{a}_j$.

Hence, the total hydrogen supply is also insufficient to realize $p^\star$. By commodity-independence of costs, any reallocation of hydrogen cannot strictly decrease the objective value, again yielding a contradiction. *Case 1b.ii:* If all arcs in p are labeled, two cases remain. Either (i) $\tilde{a}_j$ carries no passenger demand, or (ii) the passenger demand on $\tilde{a}_j$ is already allocated to activate transport capacity for another path. In both cases, enabling the transport capacity required by $p^\star$ on $\tilde{a}_j$ would require a reallocation of passenger demand to $\tilde{a}_j$. If the source vertex of p does not possess sufficient hydrogen supply to support rerouted demand, then the same shortage necessarily applies to $p^\star$, and the same argument via the commodity-independence of costs as before holds. Otherwise, obtaining this transport capacity would require rerouting another commodity to a strictly inferior path, which is not feasible by (8).

Case 2: There is no vertex label for $p^\star$ at the end of HANLA.

Case 2a: We found $p^\star$, but did not place a vertex label for this path. This implies that the operational cost of $p^\star$ is at least as large as the cost of the path selected in the initial feasible solution, which serves as the cost bound for the corresponding commodity. Hence, $p^\star$ cannot yield a strictly better solution, contradicting the assumption that $x^\star$ is strictly better.

Case 2b: We did not find $p^\star$, because the algorithm has stopped before labeling all arcs in $p^\star$ due to the condition $\mathcal{H}_v = 0$ being fulfilled for all $v \in V$. Hence, inserting $p^\star$ into x would lead to infeasibility as $p^\star$ uses more hydrogen than the paths currently in x. Since costs are commodity-independent and arc labels in our specified order with a focus on relevant arcs for the solution, any reallocation of hydrogen to accommodate $p^\star$ cannot yield a strictly smaller objective value.

Case 2c: We did not find $p^\star$, although we labeled all arcs. Then we did not find $p^\star$ because we did not place a vertex label for some subpath $\tilde{p}$ of $p^\star$; the cost to operate $\tilde{p}$ would have exceeded the cost bound placed for the commodity $[s(\tilde{p}), t(\tilde{p})]$ associated to start and end vertex of $\tilde{p}$. For $\tilde{p}$, we are then again in Case 1 or Case 2a. □

4 Computational Experiments

This section evaluates the computational performance of the proposed solution approach. In particular, we compare running times against a general-purpose solver and assess scalability on a set of instances designed to reflect realistic network characteristics. To this end, we construct a diverse set of test instances that capture key structural properties of real-world aviation networks, including network size, demand distribution, and heterogeneity in hydrogen availability. This allows us to evaluate the practical performance of the algorithm under conditions that are representative of realistic applications.

We first describe the instance generation process and the characteristics of the test sets. We then present a detailed runtime analysis and compare the performance of our approach with a state-of-the-art solver. Finally, we provide a case study to highlight the model's practical relevance and illustrate the structural insights.

All experiments were carried out with an implementation of HANLA in the C++ programming language, available via [23]. For comparison, we also computed all instances using GUROBI 12.0.1 [15]. The experiments ran on an AMD Epyc 7742 processor clocked at up to 3.40 GHz, with a time limit of 3600 s for all computations. Each individual computation was carried out by a single-threaded process.

4.1 Instances

To construct instances for the HANP, we use data from different sources, summarized in Table 1. The network is modeled as a directed graph (V, A) with a subset of 88 European airports as vertices V, including the largest airports with respect to aircraft movement based on [36], and their possible flight legs as arcs A. Commodities are defined as all origin–destination pairs of vertices $\{\{O_1, D_1\}, \ldots, \{O_N, D_N\}\}$, with demand values d_i estimated using a neural network approach [41]: The passenger demand values are derived from a data-driven framework based on publicly available data, in which machine learning techniques extend traditional gravity-model features to estimate origin–destination flows. Each airport is equipped with a hydrogen capacity $\mathcal{H}_v$, derived from a system dynamics model [36], which also computes the hydrogen market penetration Q. The system dynamics model captures interactions between airlines, airports, and aircraft manufacturers, including feedback effects in technology adoption and infrastructure provision. The hydrogen tank sizes per passenger are assumed at $\mathcal{T} = 18\,\text{kg/passenger}$; the value was converted from the total tank size in the design study of a regional jet [32].

Fuel consumption on each leg is obtained following [18], differentiating between kerosene- and hydrogen-based aircraft. A uniform seat load factor of 0.8 is applied across all scenarios. Kerosene consumption rates are set at 1.22, 2.75, and 6 kg/km for regional, short-haul, and medium-haul flights, respectively,

Table 1: Overview of the model parameters used in the formulation of the HANP

Parameter	Name	Source
Airports	V	[36]
Flight legs	A	(subset of) all possible connections
Commodities	$\{\{O_1, D_1\}, \ldots, \{O_N, D_N\}\}$	all possible connections
Demand	$d_i,\ i \in [N]$	neural network in [41]
H_2-consumption per passenger/flight leg	r_a	[18]
H_2-capacity per airport	$\mathcal{H}_v$	[36]
H_2-tank size per passenger	$\mathcal{T}$	converted from [32]
Gaseous cost for H_2	c_v^h	[36]
Non-fuel DOC for H_2-aircraft	c_a^m	[18]
H_2-market penetration	Q	[36]

Table 2: Comparison of hydrogen cost structures across scenarios (aggregated by cost levels)

	Heterogeneous scenario		**Homogeneous scenario**	
Cost range (USD/kgH_2)	**Airports**	**Capacity share** (%)	**Airports**	**Capacity share** (%)
< 4	6	24.1	1	4.3
$4 - 5$	28	55.3	61	78.6
$5 - 7$	34	18.7	20	14.8
$7 - 10$	8	1.5	3	1.2
> 10	9	0.4	3	1.1
Total	85	100	88	100

Note: The difference in the number of airports across scenarios results from missing data in [36].

with seating capacities of 60, 172, and 263 passengers. Hydrogen aircraft are modeled by applying consumption multipliers of 0.36, 0.40, and 0.42 to the kerosene benchmarks, and by reducing seating capacities to 48, 137, and 210 passengers.

Hydrogen cost inputs are derived from [36] with the non-fuel direct operating cost c_a^m taken from [18]. As the underlying data provide projections at a limited temporal resolution, we adopt the projected 2050 cost levels as static inputs across all experiments. To account for uncertainty in future hydrogen supply conditions, we consider two scenario settings that differ in their spatial cost structure for hydrogen. Table 2 summarizes the distribution of airports across different hydrogen cost ranges by reporting, for each range, both the number of airports and the corresponding capacity share, where the latter denotes the fraction of the total available hydrogen supply capacity in the network that lies within the respective cost interval. In the first (heterogeneous) scenario, hydrogen supply costs vary substantially across locations, with only a small subset of airports achieving costs below 4 USD/kgH2 and a considerable share of capacity distributed across higher cost ranges. In contrast, the second (more homogeneous) scenario is characterized by a pronounced concentration of hydrogen costs in the 4 USD/kgH2 to 5 USD/kgH2 range, which accounts for the majority of both airports and available capacity, while low-cost supply remains limited. These structural differences in the cost distribution lead to markedly different levels of hydrogen-powered aviation adoption, as shown in [36]. In particular, the heterogeneous scenario results in a relatively low market penetration of 8 %, while the more homogeneous cost structure enables a substantially higher penetration of 46 %.

To analyze how hydrogen aviation emerges under different economic conditions, we evaluate both scenarios across a range of kerosene costs (in USD/kg), specifically $\{1.60, 1.65, 1.70, 1.75, 1.80, 1.85, 1.90, 1.95, 2.00\}$. This allows us to assess the sensitivity of network structure and technology adoption to relative fuel cost levels.

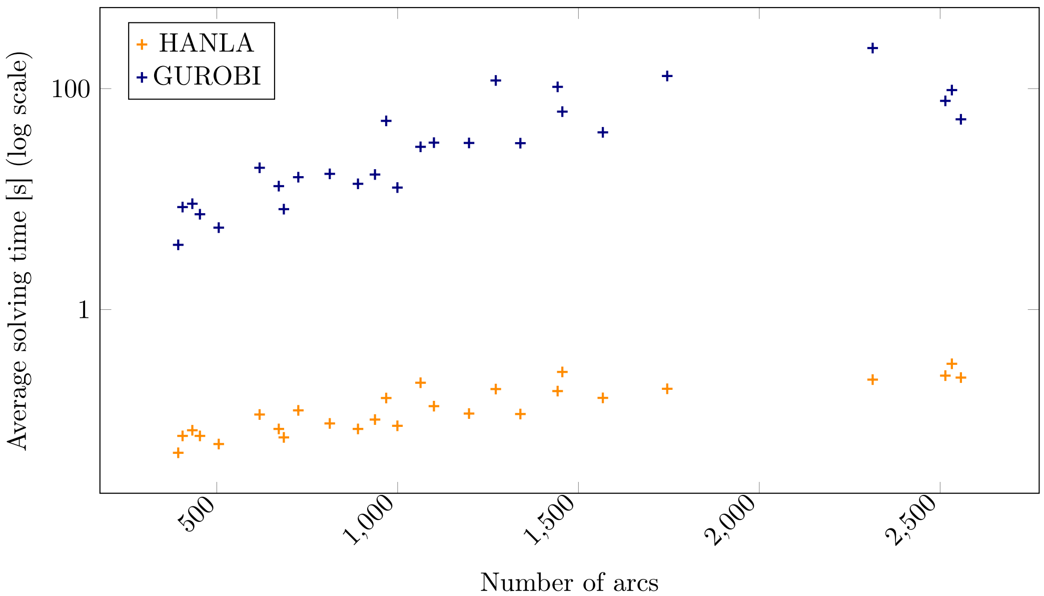

Figure 1: Comparison of the average solving time of HANLA and GUROBI, restricted to instances that were solved within the time and memory usage limit

In addition to the full-scale network instances, smaller benchmark instances are created to assess algorithmic performance at different levels of complexity. These reduced instances are derived using a deterministic random generator that decides which airports and flight legs are included, based on predefined shares of the full network. To ensure both variety and reproducibility, we apply all combinations of the shares {0.4, 0.7, 1} for airports, flight legs and number of considered commodities.

4.2 Computational Performance

We evaluated the computational performance of HANLA on a test set of 486 instances with varying network sizes. The number of airports ranges from 22 to 88, the number of edges from 197 to 7656, and the number of commodities from 202 to 9744, thereby covering sparse as well as fully dense topologies. For comparability across instances, if the hydrogen demand data from [36] indicates zero demand, a small randomly generated demand was assigned to these airports. This guarantees that all airports are active in the input and avoids discrepancies in instance definition that would otherwise distort scaling behavior. These instance sizes already illustrate the strong memory footprint of the model, emphasizing that memory-efficient formulations are crucial for scaling to realistic, large-scale network settings.

To benchmark HANLA against a general-purpose solver, the same set of instances was also solved using GUROBI, with a memory usage limit of 20 GB and time limit of one hour enforced. Out of all instances, 262 could not be solved within this memory bound and are therefore excluded from Figure 1, along with 4 instances that were not solvable within the imposed time limit both by GUROBI and HANLA.

A comparison of the solving times for GUROBI and HANLA highlights a clear difference in computational performance across the instance set. In general, HANLA is substantially faster for all instances solvable by GUROBI, often by one to two orders of magnitude. The results on memory usage, presented in Figure 2, reinforce this observation: GUROBI generally consumes more than 1 GB of RAM for most solved instances, whereas HANLA rarely exceeds 100 MB. Together, these findings indicate that HANLA is notably more efficient in both time and memory, while the performance of both solvers remains sensitive to the structural and combinatorial complexity inherent to individual instances.

We now focus solely on the computational performance of HANLA. Table 3 summarizes the results by reporting solution times, the average number of generated vertex labels, and memory consumption across all instances solved within the one-hour time limit. The values are averaged over all considered cost levels for each corresponding share of commodities, flight legs, and airports, ensuring a consistent comparison across instance classes. In total, only four instances could not be solved within the prescribed time limit, all occurring in the heterogeneous scenario—three at a kerosene cost level of 2.00 USD/kg and one at 1.95 USD/kg. This pattern can be attributed to an increase in generated vertex labels as kerosene

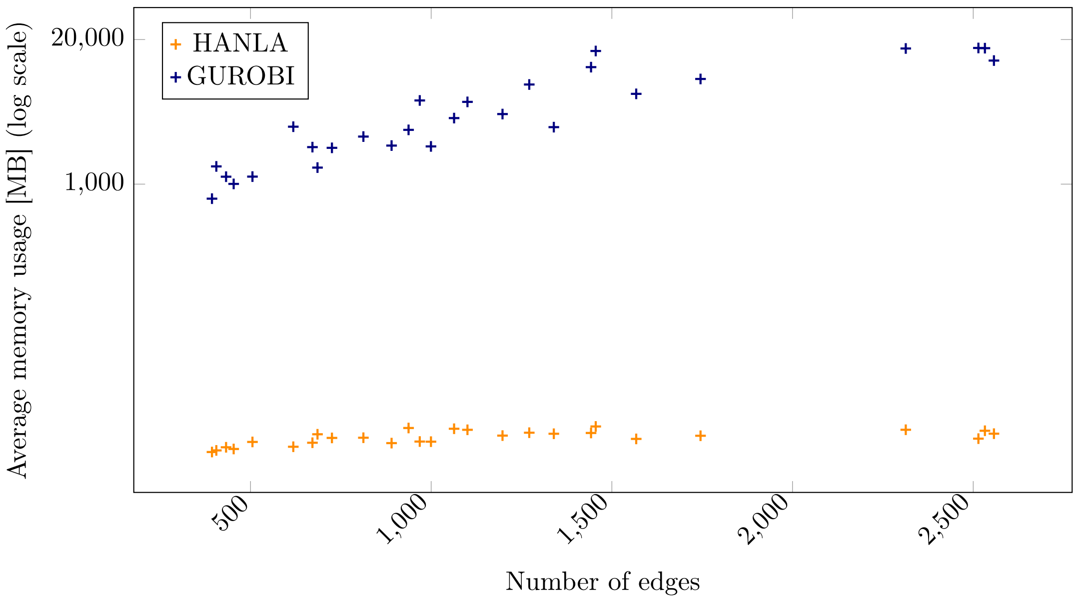

Figure 2: Comparison of the average memory usage of HANLA and GUROBI, with memory usage limit of 20 GB

costs rise, which leads to a larger and more complex search space and consequently higher computational effort.

The results in Table 3 illustrate the computational scalability of the proposed labeling algorithm as a function of problem size, measured by the share of commodities, flight legs, and airports. Across all instances, the number of generated vertex labels increases rapidly with network density, reflecting the combinatorial growth of feasible path alternatives. In particular, instances with full network size $(1.00, 1.00, 1.00)$ generate up to 34 925 labels, compared to only 24 labels in the smallest setting. This growth is primarily driven by the expansion of the flight leg and airport sets, which significantly enlarge the feasible path space, whereas increasing the number of commodities has a more moderate impact. Despite this, solution times remain tractable across all configurations, ranging from 0.07 s for small instances to approximately 128.14 s for the largest case. Memory usage exhibits a similar but well-controlled increase, remaining below 18 MB even in the largest instances. Overall, the results demonstrate that, although the labeling effort grows substantially with network size, the proposed algorithm scales efficiently and maintains practical running times, highlighting its suitability for large-scale network instances with multiple commodities and resource constraints.

In summary, HANLA exhibits robust computational performance across all tested network sizes and solves the vast majority of instances within practical running times. While the number of generated vertex labels grows rapidly with increasing network density, this growth remains computationally manageable, with solution times below 130 s and moderate memory usage. Only four instances could not be solved within the prescribed time limit. Consequently, label proliferation remains the primary driver of computational effort and becomes most pronounced in instances with complex cost structures, but does not constitute a limiting bottleneck for the majority of cases, indicating strong scalability of the proposed approach.

4.3 Case Study Results

This subsection analyzes the utilization of hydrogen infrastructure across the scenarios, focusing on the distinction between airports that are *served* by hydrogen-powered flights and those at which hydrogen capacity is actually *consumed*. This distinction is central to the model, as multi-leg refueling enables hydrogen to be transported across the network, thereby decoupling operational presence from local infrastructure availability. Figure 3 illustrates the resulting flight networks.

In the heterogeneous demand setting, hydrogen adoption increases progressively with rising kerosene cost levels. At a kerosene cost of 1.6 USD/kg, only 0.59 % of total demand is served by hydrogen (520,036 passengers). Although 23 out of 86 airports are already served by hydrogen-powered flights, hydrogen is procured at only a single airport, namely Frankfurt Airport, indicating that early operations are

Table 3: Number of created vertex labels, solving time, and RAM-memory usage of HANLA, averaged over all kerosene cost levels

share of (commodities, arcs, airports)	#vertex label	solving time (s)	mem. usage (MB)
(0.40, 0.40, 0.40)	24	0.06	4.33
(0.40, 0.40, 0.70)	254	0.19	5.77
(0.40, 0.40, 1.00)	1192	0.54	7.41
(0.70, 0.40, 0.40)	149	0.08	4.21
(0.70, 0.40, 0.70)	1031	0.30	5.67
(0.70, 0.40, 1.00)	5144	2.11	8.92
(1.00, 0.40, 0.40)	31	0.09	4.17
(1.00, 0.40, 0.70)	1924	0.61	6.81
(1.00, 0.40, 1.00)	13831	12.81	11.56
(0.40, 0.70, 0.40)	51	0.08	5.14
(0.40, 0.70, 0.70)	695	0.31	5.83
(0.40, 0.70, 1.00)	4599	2.25	8.83
(0.70, 0.70, 0.40)	361	0.11	5.21
(0.70, 0.70, 0.70)	2335	0.65	6.46
(0.70, 0.70, 1.00)	17240	21.81	12.29
(1.00, 0.70, 0.40)	47	0.11	5.43
(1.00, 0.70, 0.70)	5262	3.20	7.49
(1.00, 0.70, 1.00)	22633	44.74	14.08
(0.40, 1.00, 0.40)	89	0.10	5.24
(0.40, 1.00, 0.70)	1758	0.67	6.64
(0.40, 1.00, 1.00)	21675	62.14	13.35
(0.70, 1.00, 0.40)	629	0.17	5.87
(0.70, 1.00, 0.70)	11643	16.18	8.98
(0.70, 1.00, 1.00)	33130	101.22	17.00
(1.00, 1.00, 0.40)	66	0.13	5.74
(1.00, 1.00, 0.70)	21940	109.16	12.35
(1.00, 1.00, 1.00)	34925	114.67	17.73

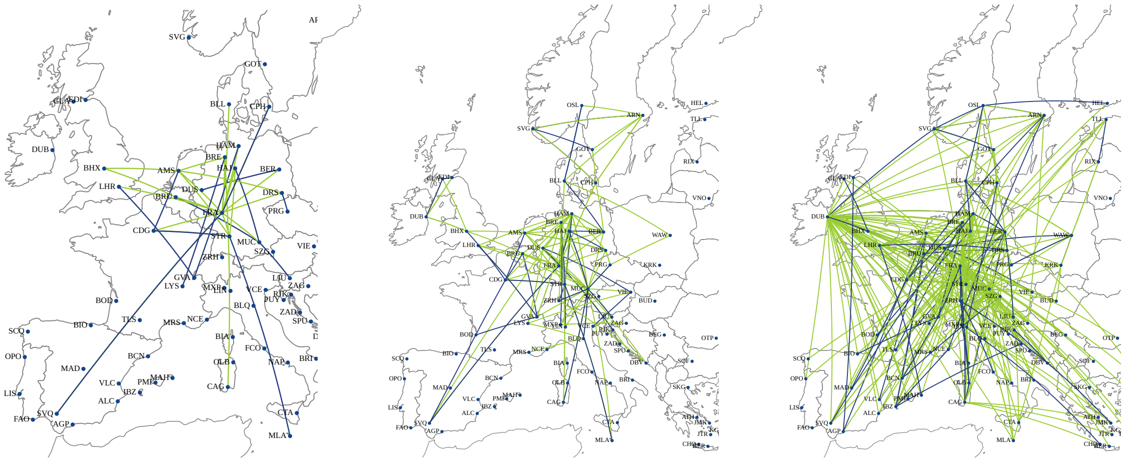

(a) 1.60 USD/kg (b) 1.75 USD/kg (c) 1.90 USD/kg

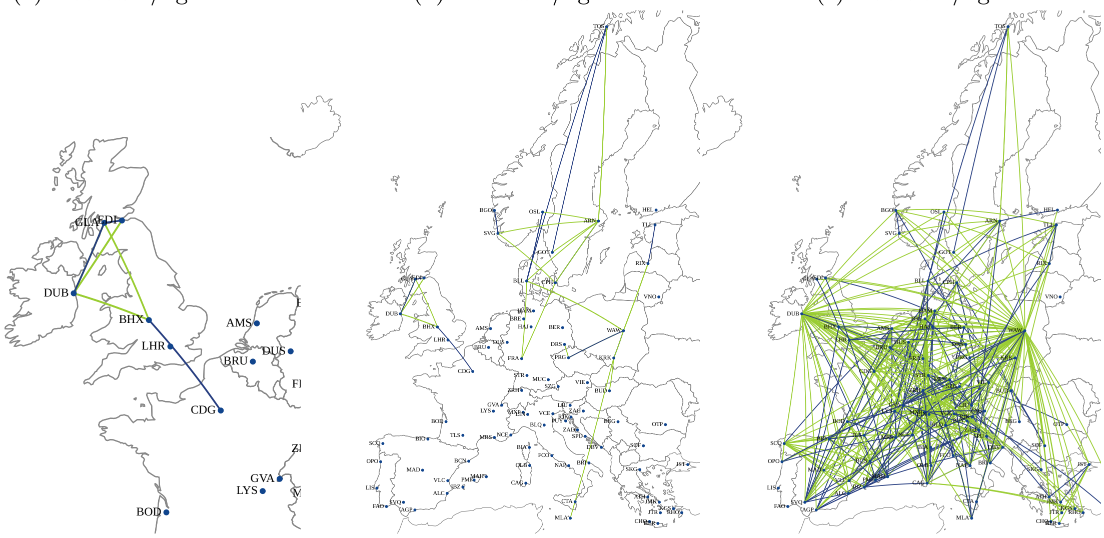

(d) 1.75 USD/kg (e) 1.90 USD/kg (f) 2.00 USD/kg

Figure 3: Hydrogen-powered European flight networks across varying kerosene cost scenarios (in USD/kg), (a)-(c) heterogeneous scenario, (d)-(f) homogeneous scenario. Connections in green utilize the full market penetration, connections in blue do not.

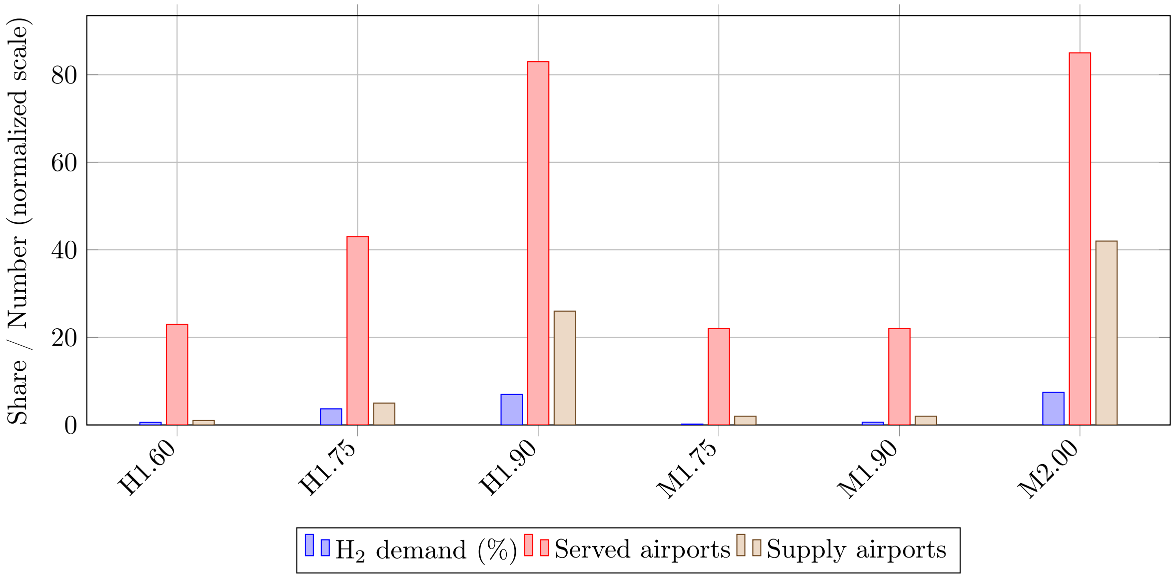

Figure 4: Hydrogen adoption and network structure across kerosene cost levels and demand scenarios. H denotes the heterogeneous scenario and M the homogeneous.

almost entirely enabled through transported hydrogen rather than local production. As kerosene cost increase (1.75 USD/kg and 1.90 USD/kg), hydrogen demand rises to 3.68 % and 6.97 %, respectively, while the number of served airports expands from 43 to 83. In contrast, the number of airports at which hydrogen is actually consumed increases more moderately from 5 to 26. This divergence highlights that hydrogen is increasingly redistributed through multi-leg itineraries, rather than being consumed locally, and underscores the importance of transport capacity in enabling system-wide feasibility. At higher adoption levels, capacity constraints become binding at several major hubs, including Frankfurt, Hamburg, and Munich, reflecting localized scarcity in high-demand regions.

A similar but structurally more concentrated pattern emerges in the homogeneous demand setting. At 1.75 USD/kg and 1.90 USD/kg for kerosene, hydrogen adoption remains limited, with shares of 0.20 % and 0.63 %, respectively. While up to 22 airports are served, hydrogen is procured at only 1–3 locations, indicating an even stronger reliance on transported hydrogen. Early adoption is concentrated on a small set of short-haul routes originating from Dublin, which serves as a natural entry node due to favorable cost conditions and connectivity to the United Kingdom. At 2.00 USD/kg, hydrogen adoption increases to 7.45 %, covering 85 out of 88 airports; however, hydrogen capacity is still utilized at only 42 airports, confirming that indirect supply via network flows remains dominant. Capacity constraints emerge at airports such as Hamburg, Dublin, and Warsaw, further emphasizing the role of infrastructure scarcity in shaping network structure.

The comparison across scenarios, see Figure 4, reveals that hydrogen adoption begins earlier in the heterogeneous setting, despite a substantial share of airports exhibiting high production costs. This is driven by the presence of a small number of low-cost supply nodes (24.1 % of capacity below 4 USD/kgH2), which act as early entry points for hydrogen operations. In contrast, the homogeneous scenario exhibits a more compressed but uniformly higher cost structure, with 78.6 % of capacity concentrated in the 4 USD/kgH2 to 5 USD/kgH2 range. The absence of strongly differentiated low-cost nodes delays the onset of hydrogen adoption, as large-scale deployment only becomes feasible once a sufficiently large portion of the network becomes jointly economically viable. These results highlight that cost heterogeneity accelerates early adoption through localized entry points, whereas cost homogeneity delays diffusion despite similar average cost levels.

4.3.1 Discussion

Overall, the results demonstrate that hydrogen-powered operations are spatially far more extensive than local hydrogen production would suggest. The persistent gap between served airports and airports with active hydrogen procurement provides direct evidence that transport capacity is systematically exploited within the network. This mechanism is particularly important in early stages of adoption, when sparse infrastructure necessitates multi-leg redistribution of hydrogen, but remains relevant even at higher penetration levels.

From a policy perspective, the findings indicate that substantial hydrogen uptake only occurs at elevated kerosene cost levels, well above current levels of approximately 1 USD/kg. Achieving meaningful adoption would therefore require either significant increases in fossil fuel prices or targeted support mechanisms for hydrogen production and infrastructure deployment. Importantly, such interventions would not only affect aggregate adoption levels but also reshape the spatial distribution of infrastructure usage, as higher penetration intensifies capacity constraints at key airports. Coordinated policy designs that jointly address cost signals and infrastructure provision are therefore essential for enabling a system-wide transition.

From a methodological standpoint, these outcomes can be interpreted as a decentralized flow allocation induced by the underlying labeling algorithm. The algorithm identifies cost-minimal feasible paths under resource constraints, where hydrogen availability acts as a binding resource along routes. The resulting solution can be viewed as an equilibrium flow pattern in which demand is routed over kerosene- and hydrogen-based paths subject to capacity, range, and market penetration constraints. Airports with binding hydrogen capacity correspond to nodes with high shadow prices, where additional supply would yield the largest marginal reduction in system costs. Conversely, the absence of dominant hub structures at higher adoption levels reflects decreasing marginal congestion effects as hydrogen becomes more widely available.

5 Conclusion and Future Work

In this paper, we introduced the Hydrogen Aviation Network Problem (HANP), an integrated multi-commodity network optimization model that jointly captures passenger flows, heterogeneous aircraft technologies, and endogenous hydrogen infrastructure availability. By explicitly incorporating multi-leg refueling operations, the model accounts for a critical operational feature of hydrogen aviation under sparse infrastructure conditions. This integrated formulation enables a system-level analysis of how infrastructure constraints and operational limitations jointly shape feasible network configurations, but results in a problem of high combinatorial complexity that is not tractable with standard solution methods at realistic scales.

To address this challenge, we developed the Hydrogen Aviation Network Labeling Algorithm (HANLA), a customized exact dynamic programming labeling approach that exploits key structural properties of HANP. In contrast to standard multi-commodity solution approaches based on column generation combined with labeling, HANLA reduces the solution process to a single labeling algorithm, avoiding the need for a master problem while maintaining optimality guarantees. Computational experiments demonstrate that HANLA substantially outperforms general-purpose solvers in both runtime and scalability, enabling the solution of networks with thousands of edges and multiple demand commodities.

Beyond computational performance, the model provides insights into the emergence of hydrogen aviation under exogenous fuel cost and supply conditions. Hydrogen adoption remains negligible at low kerosene prices but increases sharply with rising fuel costs, from below 0.6 % in early heterogeneous settings to up to 7.5 % in high-cost scenarios, while homogeneous cost structures systematically delay adoption despite lower average cost levels. Across all settings, hydrogen operations become geographically widespread, yet hydrogen procurement remains highly concentrated, with most early-stage operations relying on multi-leg refueling rather than local production. Even at high penetration levels, binding capacity constraints persist at key airports, indicating that infrastructure scarcity continues to shape equilibrium flow patterns. The resulting network evolution is characterized by a transition from localized, supply-driven entry nodes to partially diffused but structurally constrained adoption patterns. Overall, the results highlight a central trade-off in hydrogen aviation: network-wide feasibility is already enabled through multi-leg refueling under sparse infrastructure, but large-scale adoption is fundamentally governed by a small number of supply-constrained nodes. This underscores that hydrogen aviation is less a gradual diffusion process than a capacity-limited network equilibrium shaped by a few critical bottlenecks.

From a methodological perspective, our results illustrate how exploiting problem-specific structure can yield scalable and exact solution methods for complex network optimization problems that are otherwise intractable. The proposed modeling and solution approach is applicable beyond aviation, in particular to transportation systems in which flows, technology choices, and scarce infrastructure are tightly coupled.

The analysis is subject to several limitations that should be considered when interpreting the results. First, the model does not capture intertemporal dynamics in infrastructure deployment or fleet renewal, and therefore abstracts from potential path dependencies and feedback effects between demand, costs, and infrastructure expansion. Hydrogen supply conditions are treated as exogenous and static, which prevents endogenous investment responses and learning-driven cost reductions. Second, demand is modeled as aggregated passenger flows rather than explicit aircraft-level operations. This ensures tractability but abstracts from detailed scheduling, rotation, and tail-assignment decisions, as well as stochastic effects such as booking uncertainty, load factors, and seasonality. Third, the framework assumes deterministic input parameters, including fuel prices, hydrogen costs, and network availability, and thus does not account for uncertainty or disruptions in operational or market conditions. In addition, policy instruments such as emissions pricing or fleet-level CO_2 constraints are not explicitly modeled, although they may significantly affect adoption patterns. Finally, investment decisions in infrastructure and fleet composition are exogenous, limiting the analysis of co-evolution between infrastructure rollout, costs, and adoption. Extending the framework to a dynamic, stochastic setting with endogenous investment and uncertainty represents an important direction for future research.

Acknowledgements
The authors acknowledge the financial support by the Federal Ministry of Research, Technology and Space of Germany in the framework of HyNEAT under grant no. 03SF0670B. The authors would also like to acknowledge the funding by the Deutsche Forschungsgemeinschaft (DFG, German Research Foundation) under Germany's Excellence Strategy – EXC 2163/1- Sustainable and Energy Efficient Aviation – Project-ID 390881007.

References

[1] Airbus. *ZEROe - Low Carbon Aviation - Airbus.* 2021. URL: https://www.airbus.com/en/innovation/energy-transition/hydrogen/zeroe-our-hydrogen-powered-aircraft.

[2] S. Albers, J.-A. Bühne, and H. Peters. "Will the EU-ETS Instigate Airline Network Reconfigurations?" In: *Journal of Air Transport Management* 15.1 (2009), pp. 1–6. DOI: 10.1016/j.jairtraman.2008.09.013.

[3] F. Alvelos and J. M. V. de Carvalho. "An Extended Model and a Column Generation Algorithm for the Planar Multicommodity Flow Problem". In: *Networks* 50.1 (2007), pp. 3–16. DOI: 10.1002/net.20161.

[4] M. Arras et al. "Hydrogen Integration in China's Aviation Sector: Techno-economic Optimization for Flight Network Decarbonization". In: *Resources, Conservation and Recycling* 229 (2026), p. 108834. DOI: 10.1016/j.resconrec.2026.108834.

[5] Aviation Impact Accelerator. *AIA Zero Report.* Tech. rep. University of Cambridge, 2024. URL: https://report.aiazero.org/.

[6] R. Bellman. "The Theory of Dynamic Programming". In: *Bulletin of the American Mathematical Society* 60.6 (1954), pp. 503–515. DOI: 10.1090/S0002-9904-1954-09848-8.

[7] K. Button. "The Impact of US–EU "Open Skies" Agreement on Airline Market Structures and Airline Networks". In: *Journal of Air Transport Management.* Airneth Conference 2008 Special Issue: The Impact of EU-US Open Skies 15.2 (2009), pp. 59–71. DOI: 10.1016/j.jairtraman.2008.09.010.

[8] A. Contreras et al. "Hydrogen as Aviation Fuel: A Comparison with Hydrocarbon Fuels". In: *International Journal of Hydrogen Energy* 22.10 (1997), pp. 1053–1060. DOI: 10.1016/S0360-3199(97)00008-6.

[9] J. E. Cremeans, R. A. Smith, and G. R. Tyndall. "Optimal Multicommodity Network Flows with Resource Allocation". In: *Naval Research Logistics Quarterly* 17.3 (1970), pp. 269–279. DOI: 10.1002/nav.3800170303.

[10] H. Degirmenci et al. "Challenges, Prospects and Potential Future Orientation of Hydrogen Aviation and the Airport Hydrogen Supply Network: A State-of-Art Review". In: *Progress in Aerospace Sciences.* Special Issue on Green Aviation 141 (2023), p. 100923. DOI: 10.1016/j.paerosci.2023.100923.

[11] M. Desrochers. *An Algorithm for the Shortest Path Problem with Resource Constraints.* École des hautes études commerciales, Groupe d'études et de recherche en . . ., 1988.

[12] E. W. Dijkstra. “A Note on Two Problems in Connexion with Graphs”. In: *Numerische Mathematik* 1.1 (1959), pp. 269–271. DOI: 10.1007/BF01386390.

[13] H. Fan et al. “A Novel Method for Solving the Multi-Commodity Flow Problem on Evolving Networks”. In: *Computer Networks* 247 (2024), p. 110451. DOI: 10.1016/j.comnet.2024.110451.

[14] D. Feillet et al. “An Exact Algorithm for the Elementary Shortest Path Problem with Resource Constraints: Application to Some Vehicle Routing Problems”. In: *Networks* 44.3 (2004), pp. 216–229. DOI: 10.1002/net.20033.

[15] Gurobi Optimization, LLC. *Gurobi Optimizer Reference Manual*. 2026. URL: https://www.gurobi.com.

[16] T. Hintsch and S. Irnich. “Exact Solution of the Soft-Clustered Vehicle-Routing Problem”. In: *European Journal of Operational Research* 280.1 (2020), pp. 164–178. DOI: 10.1016/j.ejor.2019.07.019.

[17] J. Hoelzen et al. “H2-Powered Aviation – Optimized Aircraft and Green LH2 Supply in Air Transport Networks”. In: *Applied Energy* 380 (2025), p. 124999. DOI: 10.1016/j.apenergy.2024.124999.

[18] J. Hoelzen et al. “Hydrogen-Powered Aviation and Its Reliance on Green Hydrogen Infrastructure – Review and Research Gaps”. In: *International Journal of Hydrogen Energy*. Hydrogen Energy and Fuel Cells 47.5 (2022), pp. 3108–3130. DOI: 10.1016/j.ijhydene.2021.10.239.

[19] K. Holmberg and D. Yuan. “A Multicommodity Network-Flow Problem with Side Constraints on Paths Solved by Column Generation”. In: *INFORMS Journal on Computing* 15.1 (2003), pp. 42–57. DOI: 10.1287/ijoc.15.1.42.15151.

[20] International Civil Aviation Organization. *ICAO Environmental Report 2025*. Tech. rep. 2025. URL: https://www.icao.int/environmental-protection/envrep2025.

[21] M. Lawrence-Griffiths, D. A. Timmis, and D. C. Morton. “Modelling Hydrogen Adoption in the United States Aviation Industry through Integration of Green Hydrogen Hubs”. In: *Journal of the Air Transport Research Society* 5 (2025), p. 100079. DOI: 10.1016/j.jatrs.2025.100079.

[22] D. S. Lee et al. “The Contribution of Global Aviation to Anthropogenic Climate Forcing for 2000 to 2018”. In: *Atmospheric Environment* 244 (2021), p. 117834. DOI: 10.1016/j.atmosenv.2020.117834.

[23] L.-M. Manke. *Hydrogen-Powered Route Selection in European Air Traffic*. 2026. URL: https://github.com/lismanke/hydrogen_route_selection.

[24] L.-M. Manke and I. Joormann. “Hydrogen-Powered Aviation: An Optimization Approach Deciding on Where to Incorporate Hydrogen into the Air Traffic Sector”. In: *International Conference on Operations Research*. Springer, 2023, pp. 367–373.

[25] M. Marksel et al. “Hydrogen Infrastructure and Logistics in Airports”. In: *Fuel Cell and Hydrogen Technologies in Aviation*. Ed. by C. O. Colpan and A. Kovač. Sustainable Aviation. Springer International Publishing, 2022, pp. 117–146. ISBN: 978-3-030-99018-3. DOI: 10.1007/978-3-030-99018-3_6.

[26] L. Metz et al. “Delay-Resistant Robust Vehicle Routing with Heterogeneous Time Windows”. In: *Computers & Operations Research* 164 (2024), p. 106553. DOI: 10.1016/j.cor.2024.106553.

[27] T. R. Miller, M. Chertow, and E. Hertwich. “Liquid Hydrogen: A Mirage or Potent Solution for Aviation’s Climate Woes?” In: *Environmental Science & Technology* 57.26 (2023), pp. 9627–9638. DOI: 10.1021/acs.est.2c06286.

[28] M. Noorafza et al. “Airline Network Planning Considering Climate Impact: Assessing New Operational Improvements”. In: *Applied Sciences* 13.11 (2023), p. 6722. DOI: 10.3390/app13116722.

[29] K. Oesingmann, W. Grimme, and J. Scheelhaase. “Hydrogen in Aviation: A Simulation of Demand, Price Dynamics, and CO2 Emission Reduction Potentials”. In: *International Journal of Hydrogen Energy* 64 (2024), pp. 633–642. DOI: 10.1016/j.ijhydene.2024.03.241.

[30] P.-J. Proesmans et al. “Aircraft Design Optimization Considering Network Demand and Future Aviation Fuels”. In: *AIAA AVIATION 2023 Forum*. AIAA AVIATION Forum. American Institute of Aeronautics and Astronautics, 2023. DOI: 10.2514/6.2023-4300.

[31] A. Rau, E. Stumpf, and M. Gelhausen. “Modelling the Impact of Introducing First-Generation Narrowbody Hydrogen Aircraft on the Passenger Air Transportation Network in Europe”. In: *Journal of the Air Transport Research Society* 3 (2024), p. 100029. DOI: 10.1016/j.jatrs.2024.100029.

[32] S. Roscher, A. Gobbin, and A. Bardenhagen. "Feasibility Study on the Use of Hydrogen as an Alternative Fuel for Conventional Passenger Aircraft". In: *CEAS Aeronautical Journal* (2026), pp. 1–21.

[33] T. Rötger et al. "Reduction of the Environmental Impact of Aviation via Optimisation of Aircraft Size/Range and Flight Network". In: *IOP Conference Series: Materials Science and Engineering* 1226.1 (2022), p. 012045. DOI: 10.1088/1757-899X/1226/1/012045.

[34] A.-K. Rothenbächer, M. Drexl, and S. Irnich. "Branch-and-Price-and-Cut for the Truck-and-Trailer Routing Problem with Time Windows". In: *Transportation Science* (2018). DOI: 10.1287/trsc.2017.0765.

[35] K. Salimifard and S. Bigharaz. "The Multicommodity Network Flow Problem: State of the Art Classification, Applications, and Solution Methods". In: *Operational Research* 22.1 (2022), pp. 1–47. DOI: 10.1007/s12351-020-00564-8.

[36] F. Schenke et al. *Hydrogen Supply Networks' Evolution for Air Transport – Final Project Report.* Tech. rep. Hannover: Institutionelles Repositorium der Leibniz Universität Hannover, 2025. DOI: 10.15488/20037.

[37] G. Sirtori and L. Trainelli. "From Potential Routes to Climate Impact: Assessing the Fleet Transition to Hydrogen-Powered Aircraft". In: *Aerospace* 12.12 (2025), p. 1075. DOI: 10.3390/aerospace12121075.

[38] S. Speizer et al. "Integrated Assessment Modeling of a Zero-Emissions Global Transportation Sector". In: *Nature Communications* 15.1 (2024), p. 4439. DOI: 10.1038/s41467-024-48424-9.

[39] M. Sun et al. "A Multi-Emission-Driven Efficient Network Design for Green Hub-and-Spoke Airline Networks". In: *IET Intelligent Transport Systems* 18.2 (2024), pp. 346–376. DOI: 10.1049/itr2.12455.

[40] C. Tilk, M. Drexl, and S. Irnich. "Nested Branch-and-Price-and-Cut for Vehicle Routing Problems with Multiple Resource Interdependencies". In: *European Journal of Operational Research* 276.2 (2019), pp. 549–565. DOI: 10.1016/j.ejor.2019.01.041.

[41] A. M. Tillmann, I. Joormann, and S. C. L. Ammann. "Reproducible Air Passenger Demand Estimation". In: *Journal of Air Transport Management* 112 (2023), p. 102462. DOI: 10.1016/j.jairtraman.2023.102462.

[42] A. Trivella et al. "The Multi-Commodity Network Flow Problem with Soft Transit Time Constraints: Application to Liner Shipping". In: *Transportation Research Part E: Logistics and Transportation Review* 150 (2021), p. 102342. DOI: 10.1016/j.tre.2021.102342.

[43] P. Su-ungkavatin, L. Tiruta-Barna, and L. Hamelin. "Biofuels, Electrofuels, Electric or Hydrogen?: A Review of Current and Emerging Sustainable Aviation Systems". In: *Progress in Energy and Combustion Science* 96 (2023), p. 101073. DOI: 10.1016/j.pecs.2023.101073.

[44] R. D. Wollmer. "Multicommodity Networks with Resource Constraints: The Generalized Multicommodity Flow Problem". In: *Networks* 1.3 (1971), pp. 245–263. DOI: 10.1002/net.3230010304.

[45] J. Wu et al. "Optimizing Hydrogen-Powered Aircraft Fleet Operations: A Mixed Integer Optimization Approach with Carbon Emission Consideration". In: *2023 Asia-Pacific International Symposium on Aerospace Technology (APISAT 2023) Proceedings.* Ed. by S. Fu. Springer Nature, 2024, pp. 174–188. ISBN: 978-981-97-3998-1. DOI: 10.1007/978-981-97-3998-1_15.

[46] R. Yan et al. "Sustainable Aviation Fuel and Next-Generation Aircraft: Low-carbon Pathway for China's Civil Aviation Industry". In: *Journal of Environmental Management* 391 (2025), p. 126493. DOI: 10.1016/j.jenvman.2025.126493.

[47] S. Yuan and S. Ming. "Evaluating Hydrogen Technology Adoption in Airlines: A Game Theory Approach to Achieving Carbon Neutrality in Airlines by 2050". In: *Materials Today Sustainability* 33 (2026), p. 101316. DOI: 10.1016/j.mtsust.2026.101316.

[48] T. Yusaf et al. "Sustainable Aviation—Hydrogen Is the Future". In: *Sustainability* 14.1 (2022), p. 548. DOI: 10.3390/su14010548.

[49] T. Yusaf et al. "Sustainable Hydrogen Energy in Aviation – A Narrative Review". In: *International Journal of Hydrogen Energy* 52 (2024), pp. 1026–1045. DOI: 10.1016/j.ijhydene.2023.02.086.

[50] M. Zanin and F. Lillo. "Modelling the Air Transport with Complex Networks: A Short Review". In: *The European Physical Journal Special Topics* 215.1 (2013), pp. 5–21. DOI: 10.1140/epjst/e2013-01711-9.